Film and Dropwise Condensation

50

John W. Rose

Contents

Abstract

The chapter covers four main areas of condensation heat transfer. The process at the vapor-liquid interface during condensation is first discussed. In many cases it is adequate to assume equilibrium at the interface but in dropwise condensation and condensation of metals the interface temperature discontinuity plays and important role. The traditional problems of laminar film condensation on plates and tubes are covered in some detail including natural and forced convection problems, the effect of vapor superheat and of the presence of non-condensing

J. W. Rose (✉)
School of Engineering and Materials Science, Queen Mary University of London, London, UK
e-mail: j.w.rose@qmul.ac.uk

F. A. Kulacki (ed.), *Handbook of Thermal Science and Engineering*,
https://doi.org/10.1007/978-3-319-26695-4_50

gases in the vapor. The specific problems of condensation on finned surfaces and in microchannels are treated in some detail. An extensive section covers dropwise condensation and incudes both experimental investigations and theory.

Nomenclature

A	Cross-sectional area of channel
$A(r)$	Distribution function; see Eq. 65
b	Spacing between fin flanks at fin tip
D	Vapor-gas diffusion coefficient
d	Diameter of tube
d_0	Tube diameter measured to fin tip
d_r	Tube diameter measured to fin root
F	Defined in Eq. 23
F_x	Defined in Eq. 17
f	Fraction of surface area covered by drops with base radius greater than r
f_f	Defined in Eq. 35
f_s	Defined in Eq. 36
G	Dimensionless quantity defined in Eq. 12, mass flux of vapor in channel
g	Specific force of gravity
h	Radial height of fin
h_v	Effective vertical height of fin; see Eqs. 40 and 41
h_{fg}	Specific latent heat of evaporation
K	Defined in Eq. 19
K_1	Constant in Eq. 47
K_2	Constant defined in Eq. 60
K_{20}	Ratio of base to curved surface area of drop; see Eq. 52
K_{21}	Defined in Eq. 62
K_3	Constant in Eq. 69
k	Thermal conductivity of condensate
L	Height of condensing surface
L_0	Defined in Eq. 57
L_3	Defined in Eq. 70
M_v	Molar mass of vapor
M_g	Molar mass of noncondensing gas
m	Interface mass flux, condensation mass flux
m_x	Local condensation mass flux
$\overline{Nu}$	Mean Nusselt number
Nu_d	Nusselt number for condensation on horizontal tube
Nu_x	Local Nusselt number
$N(r)$	Distribution function; see Eq. 66
P	Pressure of vapor-gas mixture
P_v	Vapor pressure

p	Perimeter of channel
$P_{\text{sat}}(T_v)$	Saturation temperature at T_v
$P_{\text{sat}}(T_0)$	Saturation temperature at T_0
n	Constant in Eq. 64
Q	Heat flux
Q_1	Defined in Eq. 58
Q_2	Defined in Eq. 59
Q_{21}	Value of Q_2 for steam at $T_{sat} = 373.15$ K, i.e., $Q_{21} = 2.556$ GW/m^2
$q, \overline{q}$	Heat flux, mean heat flux for surface
q_b	Mean heat flux at base of drop
q_i	Mean heat flux at curved surface of drop
q_{Nu}	Heat flux given by Nusselt theory
q^*	Dimensionless heat flux defined in Eq. 72
R	Specific ideal-gas constant
Re_x	Reynolds number, $U_\infty \rho_v x/\mu_v$
Re_d	Reynolds number, $U_\infty \rho_v d/\mu_v$
$\tilde{R}\text{e}_x$	Two-phase Reynolds number, $U_\infty \rho x/\mu$
$\tilde{R}e_d$	Two-phase Reynolds number, $U_\infty \rho d/\mu$
r	Base radius of drop
r_c	Radius of curvature of condensate surface, radius of curved surface of drop
$r_{\max}$	Effective mean base radius of largest drop
$r_{\min}$	Base radius of smallest viable drop
Sc	Schmidt number, $\mu_v/\rho_v D$
Sp	Defined in Eq. 26
s	Spacing between fin flanks at fin root
T_{v}	Vapor temperature
T_{w}	Wall temperature
T_{sat}	Saturation temperature
$T_{1\text{sat}}$	373.15 K
T_0	Vapor-liquid interface temperature
T^*	Reference temperature
T_{t}	Defined in Eq. 37
T_{f}	Defined in Eq. 38
T_{s}	Defined in Eq. 39, saturation temperature
t	Fin thickness at tip
t_p	Promoter layer thickness
U_∞	Vapor or vapor-gas mixture free stream velocity
u	Condensate streamwise velocity
v_f	Specific volume of saturated liquid
v_g	Specific volume of saturated vapor
v_{fg}	$v_g - v_f$
W_∞	Mass fraction of noncondensing gas in the bulk
W_0	Mass fraction of noncondensing gas at the interface

X	Defined in Eq. 25
x	Coordinate along channel normal to streamwise direction
y	Coordinate normal to surface
z	Streamwise coordinate

Greek Symbols

α	Heat-transfer coefficient $q/\Delta T$
α_z	Local (averaged around perimeter) heat-transfer coefficient at distance z along channel
β	Constant in Eq. 6, half angle at fin tip in Eqs. 33, 34, 35, and 36, contact angle, channel inclination to vertical in Eq. 43.
β_x	Defined in Eq. 30
γ	Ratio of principal specific heat capacities of vapor
δ	Local condensate film thickness
ΔP	Difference between vapor pressure and saturation pressure at interface temperature
ΔT	Vapor-surface temperature difference
ΔT_c	Temperature difference attributable to conduction in drop
ΔT_i	Temperature difference attributable to interphase matter transfer
ΔT_p	Temperature difference across promoter layer
ΔT_σ	Temperature difference attributable to surface curvature
$\Delta\rho$	$\rho_f - \rho_g$
ζ	Defined in Eq. 31, defined in Eq. 45
$\varepsilon_{\Delta T}$	Enhancement ratio
θ	Celsius temperature, dimensionless temperature difference defined in Eq. 73
θ_0	Defined in Eq. 74
λ	Thermal conductivity of liquid
λ_l	Thermal conductivity of liquid
λ_p	Thermal conductivity of promoter layer
μ	Viscosity of condensate
μ_v	Viscosity of vapor or vapor-gas mixture
ν	μ/ρ
ξ	Constant in Eq. 1, function defined in Eq. 42
ρ	Density of liquid, condensate
ρ_v	Density of vapor or vapor-gas mixture
ρ_g	Density of saturated vapor
ρ_f	Density of saturated liquid
ρ_{fg}	$\rho_f - \rho_g$
$\widetilde{\rho}$	$\rho - \rho_v$
σ	Surface tension
τ_ι	Streamwise vapor shear stress at condensate surface
ϕ	Retention angle measured from top of tube

χ Vapor quality
ψ Angle between normal to channel surface and Y coordinate (see Fig. 1 of Wang and Rose 2005)
ω Defined in Eq. 29

1 Introduction

The following topics are covered:

(a) The vapor-liquid interface.
The fact that equilibrium conditions do not prevail during condensation results in a temperature drop between the bulk vapor and the liquid in the immediate vicinity of the interface. This is generally small in comparison with the temperature drop in the condensate between the interface and the solid condensing surface. However, the interface temperature drop is important for condensation of metals owing to their high liquid thermal conductivity and in dropwise condensation where much of the heat-transfer takes place through extremely small droplets.

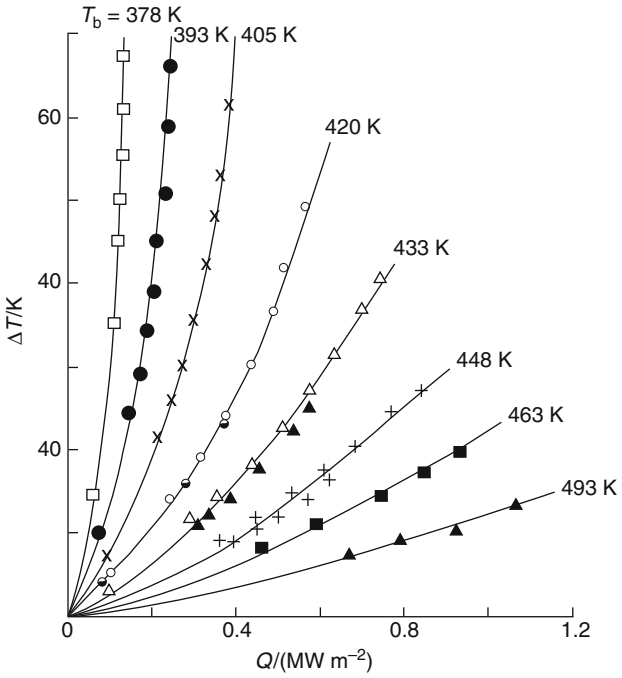

Fig. 1 Condensation of mercury at different pressures. Vapor-surface temperature difference versus heat flux (Niknejad and Rose 1981). T_b bulk vapor temperature

(b) Film condensation on smooth and finned surfaces and in small channels. Condensate films are generally very thin and film Reynolds numbers are often low so that laminar flow analysis covers a wide range of practically important problems. Effect of the presence of a noncondensing gas in the vapor is also discussed.
(c) Dropwise condensation. Dropwise condensation has recently seen a resurgence of interest and is treated in some detail. There now exists a reliable experimental heat-transfer database, and the theory is well understood. Heat-transfer coefficients are much higher than those for film condensation. However, to date no method for sustaining the dropwise mode for sufficiently long time intervals has been found, and dropwise condensation has not yet been successfully employed in practice.

2 Interface Temperature Discontinuity

In most applications, the interface temperature discontinuity is negligible in comparison with the temperature drop across the condensate but is of crucial importance in dropwise condensation and in film condensation of metals. It is also significant in condensation on low-finned tubes in cases where the condensate thermal conductivity is relatively high as in condensation of steam.

Phenomena at the vapor-liquid interface during condensation and evaporation have been investigated for many years. In kinetic theory, the liquid is regarded as having a sharply defined mathematical surface from which molecules are emitted and incident molecules from the vapor are absorbed; the problem is to obtain an (approximate) solution of the Boltzmann equation for the vapor in the immediate vicinity (a few vapor mean free paths) of the liquid surface. Account may be taken of the possibility of reflection of incident vapor molecules at the liquid surface by incorporating a *condensation coefficient*, the fraction of vapor molecules incident on the liquid surface which remains in the liquid phase. If all incident molecules remained in the liquid phase, the condensation coefficient would be unity. If in addition, and at equilibrium, the assumed Maxwellian velocity distribution in the bulk vapor persists up to the interface, then the emitted flux must also be (half) Maxwellian and may be readily calculated. If the condensation coefficient is less than unity, the evaporative flux is less than the Maxwellian value, and an *evaporation coefficient* may be defined as the ratio of the evaporative flux to the Maxwellian value. Evidentially the evaporation and condensation coefficients are equal at equilibrium.

For net evaporation or condensation, a Maxwellian distribution corresponding to the interface temperature is used for emitted molecules, and in these circumstances, the velocity distribution for the vapor immediately adjacent to the interface cannot be Maxwellian. In many approaches, the two coefficients are taken to be unity for net evaporation and condensation. For near-equilibrium conditions, and when the evaporation/condensation coefficient is taken as unity, somewhat different kinetic theory approaches for monatomic molecules give virtually identical results (see Rose 1998a) and do not differ widely from each other for significant departure from equilibrium.

Experimental investigations of both evaporation and condensation have led to a wide range of reported values of evaporation/condensation coefficients. Comparisons with kinetic theory have indicated condensation coefficients ranging from around 0.03 to unity. Knudsen (1915) reported experiments on evaporation of mercury which first indicated an evaporation coefficient of 0.0005, but, after continually increasing the purity of the mercury, a value of unity was eventually obtained with a stated experimental error of 1% (see Schrage 1953).

For low condensation rates, kinetic theory results of several investigators (Labuntsov 1967; Labuntsov and Muratova 1969; Sone and Onishi 1973; Labuntsov and Kryukov 1979; Ytrehus and Alvestad 1981; Rose 2000) indicate that the interface temperature drop and condensation mass flux are related by

$$P_{sat}(T_v) - P_{sat}(T_0) = m(RT_0)^{1/2}/\xi \tag{1}$$

where ξ depends on condensation coefficient and, when the condensation coefficient is taken as unity, varies between 0.66 and 0.67 according to the different approaches (see Rose 1998a).

For condensation of mercury the calculated interface temperature drop is much larger than that across the condensate film. Measurements of Niknejad and Rose (1981) for vapor pressures in the approximate range 50 Pa to 4 kPa are shown in Fig. 1. The calculated temperature difference across the condensate film ranged from around 0.1 K at the lowest pressure to around 3 K at the highest pressure and heat flux. It is evident that in all cases, the interface temperature drop significantly exceeds that across the condensate film. The accuracy, with which the interface temperature drop is determined by subtracting the calculated temperature drop across the condensate film from the observed vapor-surface temperature difference, is clearly little affected by the accuracy with which the condensate temperature drop is calculated, particularly at the lower pressures. These data may be used to determine values of ξ. It may be seen from Fig. 2 that values of ξ determined from these measurements may reasonably be extrapolated, for $m \rightarrow 0$, to a value around 0.66–0.67. These results provide strong evidence for the general validity of the kinetic theory model and a value of condensation coefficient near unity, at least for low condensation rates.

Note that Eq. 1 applies strictly to monatomic molecules. An "intuitively and phenomenologically" derived correction for polyatomic molecules has been given by Le Fevre (1964):

$$P_{sat}(T_v) - P_{sat}(T_0) = \frac{(\gamma+1)}{4(\gamma-1)} m(RT_s)^{1/2}/\xi \tag{2}$$

where γ is the ratio of the principal specific heat capacities for the vapor.

Equation 2 evidently agrees with Eq. 1 for monatomic molecules ($\gamma = 5/3$) and gives an increased interface temperature difference for more complex molecules with

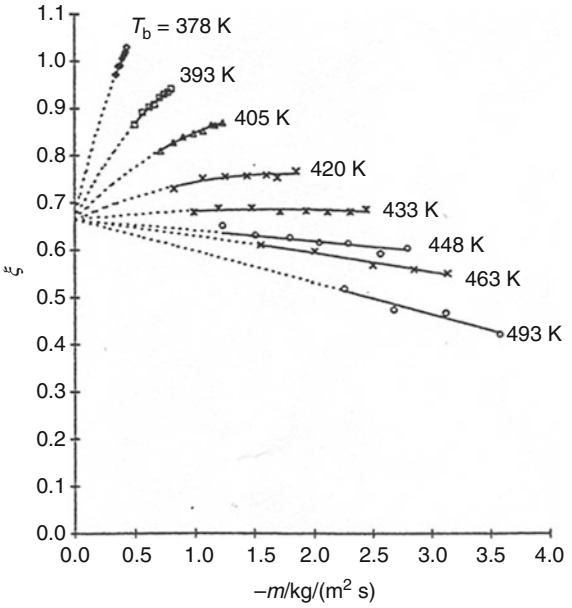

Fig. 2 Condensation of mercury at different pressures. ξ versus condensation mass flux (Niknejad and Rose 1981). Note – m here denotes *condensation* mass flux

smaller values of γ. Taking ξ as 2/3 the Clausius-Clapeyron equation with the approximation $(dP/dT)_{sat} = (\Delta P/\Delta T)_{sat}$ when $(T_v\text{-}T_0) \ll T_v$ and $q = m\, h_{fg}$, Eq. 2 gives

$$T_v - T_0 = 3qv_{fg}T_v(RT_v)^{1/2}(\gamma + 1)/8(\gamma - 1)h_{fg}{}^2 \tag{3}$$

More recently molecular dynamic simulation approaches (Nagayama and Tsuruta 2003; Wang et al. 2003; Meland et al. 2004; Ishiyama et al. 2004a, b, 2005; Tsuruta and Nagayama 2005) have been used to assess the validity of kinetic theory with reported values of evaporation/condensation coefficients. It is important to note that that these coefficients are essentially concepts adopted in the kinetic theory model to account for discrepancies between (mostly inaccurate) experiments and the model. In molecular dynamic simulation, as in reality, there is no abrupt interface, and subjective judgment (based on density distribution) is necessary to select the position for determination of an "interface temperature" appropriate for comparison with the kinetic theory model. Systematic methods adopted in molecular dynamic simulations for selecting the effective interface position have led to conclusions that the condensation coefficient is temperature dependent, falling from a value near unity to somewhat smaller values at higher temperatures. Similar conclusions have been reached in molecule tracking treatments where subjective decisions are needed on what are considered to be reflected, absorbed, and emitted molecules. Overall it seems that little more can be said with certainty than that molecular dynamic simulations lend general support to the kinetic theory model with condensation/evaporation coefficient not far from unity. For practical calculations where the interface temperature drop is thought to be important, Eq. 3 is recommended for its determination/estimation.

3 Film Condensation on Plates and Tubes

3.1 Natural Convection

The Nusselt (1916) treatment of laminar film condensation of a saturated vapor has proved remarkably successful. The key approximations are laminar boundary layer flow of the condensate film, inertia and convection terms neglected, shear stress and temperature drop at the condensate-vapor interface neglected, pressure in condensate film at given depth equal to that in the bulk vapor, and properties taken as uniform. This leads to the well-known results:

$$\overline{Nu} = \frac{\overline{q}}{\Delta T}\ \frac{L}{k} = \frac{4}{3}\left(\frac{g\ \rho\ \Delta\rho\ h_{fg}\ L^3}{4\mu\ k\ \Delta T}\right)^{1/4} = 0.943\left(\frac{g\,\rho\,\Delta\rho\,h_{fg}L^3}{\mu\,k\,\Delta T}\right)^{1/4} \tag{4}$$

for the vertical plate with uniform temperature. It may be noted that the Nusselt theory predicts an infinite local heat-transfer coefficient at the top of the plate. In cases where the coolant-side thermal resistance is substantially greater than that on the condensing side, a more suitable approximation may be that the heat flux rather than the surface temperature is uniform. This gives the same expression (Eq. 4) with uniform q and mean ΔT. For the horizontal cylinder, and with the additional approximation that the condensate film thickness is much smaller than the radius of the cylinder, numerical integration is needed to obtain:

$$\overline{Nu} = 0.728\left(\frac{g\,\rho\Delta\rho\,h_{fg}d^3}{\mu\,k\,\Delta T}\right)^{1/4} \tag{5}$$

(The leading constant in Eq. 5 is $(8/3)(2\pi)^{1/2}\Gamma(1/3)^{-9/4} = 0.728\ 018\ldots$ (Rose 1998b). It is interesting to note that Nusselt used a planimeter for integration and obtained results which give a remarkably accurate value of 0.725 for the constant in Eq. 5.) The fact that the calculated film thickness approaches infinity near the bottom of the cylinder does not lead to significant error since the heat flux there is very small. A solution for the uniform heat flux case (Fujii et al. 1972c) gives a leading constant 0.695 in Eq. 5 with a mean value of ΔT. However, in this case, the result is less accurate since the mean value of the vapor-surface temperature difference is significantly affected by the erroneous values toward the lower part of the cylinder. Measurements show that the temperature variation around the tube surface is quite well represented by a cosine function (Memory and Rose 1991) and when this is used the same expression as Eq. 5 is found with mean heat flux and mean temperature difference. Negligible effect was seen when taking account of two-dimensional conduction in the condensate film due to variation of tube surface temperature (Zhou and Rose 1996).

With the advent of digital computers, the Nusselt approximations (neglect of inertia and convection terms, effect of surface shear stress, variable properties) have

been examined by Sparrow and Gregg (1959), Koh et al. (1961), Chen (1961a, b), and others. These show the Nusselt approximations to be remarkably accurate and that errors are likely to be smaller than other uncertainties in practical problems. Various reference temperatures for property evaluation have been suggested, typically of the form:

$$T^* = T_w + \beta(T_0 - T_w) \tag{6}$$

with β in the range 0.1–0.3 according to fluid and conditions. However, in practice the choice of reference temperature used for property evaluation is not critical. The following, obtained by taking the k and ρ to vary linearly with temperature across the condensate film and $\ln(\mu)$ to vary linearly with reciprocal temperature, are suggested:

$$k = \{k(T_0) + k(T_w)\}/2 \tag{7}$$

$$\rho = \{\rho(T_0) + \rho(T_w)\}/2 \tag{8}$$

$$\mu = \mu(T^*) \text{ where } T^* = (3/4)T_w + (1/4)T_0 \tag{9}$$

with

$$h_{fg} = h_{fg}(T_0) \tag{10}$$

3.2 Forced Convection

As for free convection condensation, the uniform property laminar boundary layer equations for both vapor and condensate film, with matching conditions for velocity and shear stress at the interface, may be solved exactly using similarity transformations. For forced convection condensation, it is implicit that the shear stress from the flowing vapor on the condensate surface (insignificant in the free convection case) be included. For a horizontal flat plate, where gravity is not involved, solutions with differing degrees of approximation have been given by Cess (1960), Koh (1962), and Shekriladze and Gomelauri (1966). These are discussed in detail by Rose (1988a). For the most general solution due to Koh (1962), the results have been summarized by Rose (1989):

$$Nu_x \tilde{R}e_x^{-1/2} = 0.436\left\{\frac{1.508}{\left(1 + k\Delta T/\mu h_{fg}\right)^{3/2}} + \frac{1}{G}\right\}^{1/3} \tag{11}$$

where

$$G = \left(\frac{k\,\Delta T}{\mu\, h_{fg}}\right)\left(\frac{\rho\,\mu}{\rho_v\,\mu_v}\right)^{1/2} \tag{12}$$

In the low condensation rate limit ($G \to 0$), Eq. 11 becomes

$$Nu_x \tilde{R}e_x^{-1/2} = 0.436\, G^{-1/3} \tag{13}$$

as obtained by Cess (1960) and in the high condensation rate limit ($G \to \infty$)

$$Nu_x \tilde{R}e_x^{-1/2} = 0.5\left(1 + k\,\Delta T/\mu\, h_{fg}\right)^{-1/.2} \tag{14}$$

as obtained by Shekriladze and Gomelauri (1966). $k\,\Delta T/\mu\, h_{fg}$ is generally small (note that ΔT is the temperature drop across the condensate film and not the difference between the remote vapor and wall temperatures when the vapor is superheated or contains a noncondensing gas or the interface temperature drop is significant as for condensation of metals) so that in most cases

$$Nu_x \tilde{R}e_x^{-1/2} = 0.5 \tag{15}$$

is adequate for high condensation rates. Note that in the above expressions, the heat-transfer coefficient varies as $x^{-1/2}$ so that the mean value over distance L is twice the local value at L.

For vertical surfaces with vertical vapor downflow, both vapor shear stress and gravity play significant roles, and there is no similarity solution. Numerical solutions by Shekriladze and Gomelauri (1966) for the case of high condensation rate give:

$$Nu_x \tilde{R}e_x^{-1/2} = \frac{1}{2}\left\{\frac{1 + (1 + 16F_x)^{1/2}}{2}\right\}^{1/2} \tag{16}$$

where

$$F_x = \frac{\mu h_{fg}\, gx}{k\Delta T U_\infty{}^2} \tag{17}$$

measures the relative importance of gravity and vapor velocity. Approximate integral solutions by Fujii and Uehara (1972) for the more general case (covering both high and low condensation rates) were summarized by:

$$Nu_x \tilde{R}e_x^{-1/2} = \left(K^4 + F_x/4\right)^{1/4} \tag{18}$$

where

$$K = 0.45\left(1.2 + G^{-1}\right)^{1/3} \tag{19}$$

In the relatively rare circumstances where $k\,\Delta T/\mu\, h_{fg}$ is not small, Rose (1988a) proposed that K be amended to

$$K = 0.436\left(\frac{1.508}{\left\{1+\frac{k\Delta T}{\mu h_{fg}}\right\}^{3/2}}+\frac{1}{G}\right)^{1/3} \tag{20}$$

For forced convection condensation on a horizontal tube, solutions have been proposed by Shekriladze and Gomelauri (1966), Denny and Mills (1969), and Fujii et al. (1972b). Fujii et al. (1972b) give an expression which may be written:

$$Nu_d = \left\{0.656\left(\frac{U_\infty \rho d}{\mu}\right)^2\left(1+\left[\frac{\rho_v \mu_v}{\rho \mu}\right]^{1/2}\frac{\mu h_{fg}}{k\Delta T}\right)^{4/3}+\frac{0.276\rho^2 d^3 h_{fg} g}{\mu k \Delta T}\right\}^{1/4} \tag{21}$$

However, the problem here is complicated by vapor boundary layer separation, where the position of onset of separation is affected by the condensation mass flux. Further complication arises from the possibility of condensate film instability (Rose 1984) due to pressure variation around the tube. Details of various solutions are given by Rose (1988a). In view of the uncertainties, the relatively straightforward solution using the infinite condensation rate approximation for the surface shear stress is probably adequate. In this case, vapor boundary layer separation does not occur, and when pressure variation due to flow around the cylinder is neglected, solutions may be obtained (see Shekriladze and Gomelauri 1966) for the case of vertical vapor downflow on an isothermal tube and assuming potential flow outside the vapor boundary layer. These solutions were repeated by Lee and Rose (1982), from which Rose (1984) obtained:

$$\overline{Nu}\tilde{R}e_d^{-1/2} = \frac{0.9+0.728F^{1/2}}{\left(1+3.44F^{1/2}+F\right)^{1/4}} \tag{22}$$

where

$$F = \frac{\mu h_{fg} g d}{k \Delta T {U_\infty}^2} \tag{23}$$

Equation 22 agrees with the numerical solutions everywhere to within 0.4%. For $U_\infty = 0$ and with $\rho_{fg} \approx \rho$, Eq. 22 reduces to the Nusselt result (Eq. 5). For moderate vapor velocities (F down to around 0.1), Eq. 22 is in satisfactory agreement with data for steam (Memory and Rose 1986; Ali et al. 2013). For higher vapor velocities, Eq. 22 overestimates data for steam (Michael et al. 1989) and underestimates data for R113 (Rahbar and Rose 1984).

3.3 Effect of Vapor Superheat

The effect of vapor superheat on condensation heat-transfer is small. Minkowicz and Sparrow (1966) reported increased heat-transfer coefficients (over values obtained

from the Nusselt theory with the condensate surface temperature taken as the saturation value) of 1% and 5% for superheats of 56 K and 220 K, respectively.

3.4 Effect of Presence of a Noncondensing Gas in the Vapor

The presence of a noncondensing gas in a condensing vapor decreases the heat-transfer coefficient. This is due to the increase in gas concentration at the interface (and corresponding decrease in the partial pressure of the vapor) where the vapor is removed by condensation. Assuming equilibrium at the interface, the liquid surface temperature corresponds to the partial pressure of the adjacent vapor which is lower than that in the bulk so that the temperature drop across the condensate film is less than that between the bulk vapor and the surface. In free convection, the heat-transfer coefficient (based on bulk vapor-to-surface temperature difference) is significantly reduced by small concentrations of gas in the bulk vapor.

For free convection condensation on a vertical flat plate, boundary layer solutions have been obtained for the case where the noncondensing gas has the higher molar mass so that the condensate and vapor boundary layers both begin at the top of the plate. The vapor-gas and condensate film boundary layer equations may be solved subject to uniform bulk conditions and uniform surface temperature with interface continuity of velocity, temperature, and mass flux of the condensing constituent at the interface and when the condensate surface is impermeable to the noncondensing gas. The problem permits similarity transformations with uniform temperature and composition along the interface. Numerical solutions have been obtained by Sparrow and Lin (1964) for the uniform property case. Minkowicz and Sparrow (1966) gave more general solutions for steam-air mixtures. An approximate integral treatment of the vapor-gas boundary layer problem by Rose (1969), together with the Nusselt result for the condensate film, gives a result in the form of an algebraic equation which agrees satisfactorily with those of Sparrow and Lin (1964) and Minkowicz and Sparrow (1966). This is valid for any vapor-gas combination and has the advantage that numerical solutions are not required. The result may be expressed:

$$\begin{aligned} &10\ Sp\,Sc\left(\frac{\mu\rho}{\mu_v\rho_v}\right)\left(\frac{W_\infty}{W_0-W_\infty}\right)^2\left(\frac{20}{21}+\frac{W_0}{W_\infty}Sc\right)\\ &+\frac{8}{Sp^2Sc}\left(\frac{\mu_v\rho_v}{\mu\rho}\right)\left(\frac{W_0-W_\infty}{W_0}\right)^2\left(\frac{5}{28}Sp-\frac{X(W_0-W_\infty)}{3}\right)\\ &=\frac{100}{21}\frac{W_\infty}{W_0}-2\left(\frac{W_0-W_\infty}{W_0}\right)+8\,Sc \end{aligned} \tag{24}$$

where

$$X=\frac{M_g-M_v}{M_g-W_\infty\left(M_g-M_v\right)} \tag{25}$$

$$Sp=\frac{(T_0-T_w)k}{h_{fg}\mu} \tag{26}$$

For given bulk composition (gas mass fraction W_∞) and condensing surface temperature T_w, Eq. 24 relates the interface temperature T_0 and composition W_0 and may be solved iteratively with the condition for equilibrium at the interface

$$\frac{P_{sat}(T_0)}{P} = \frac{1 - W_0}{1 - W_0\left(1 - M_v/M_g\right)} \tag{27}$$

to determine the interface composition and temperature from which the heat-transfer coefficient may be found using the Nusselt result for the condensate film to obtain the heat flux. Suitable mean property values may be incorporated during the iterative process. Comparisons between the approximate and exact solutions are given in Figs. 3 and 4.

For forced convection condensation with parallel flow on a horizontal isothermal flat plate in the presence of a noncondensing the gas, numerical boundary layer solutions have been obtained by Koh (1962), Sparrow et al. (1967), and Fujii et al. (1977). It is seen that the normal component of velocity of the vapor at the interface (due to condensation) varies as the reciprocal of the square root of distance from the leading edge and the temperature and vapor composition are uniform along the interface. The solution of Sparrow et al. (1967), where the condensate surface velocity was neglected, is in good agreement with the more general solutions of Koh (1962) and Fujii et al. (1977). For given remote vapor composition and velocity (both independent of the streamwise coordinate), the interface temperature and composition and hence the local condensation rate and heat flux may be determined. Using existing solutions for the identical problem of heat-transfer with surface suction, Rose (1980) obtained a result in the form of an algebraic equation

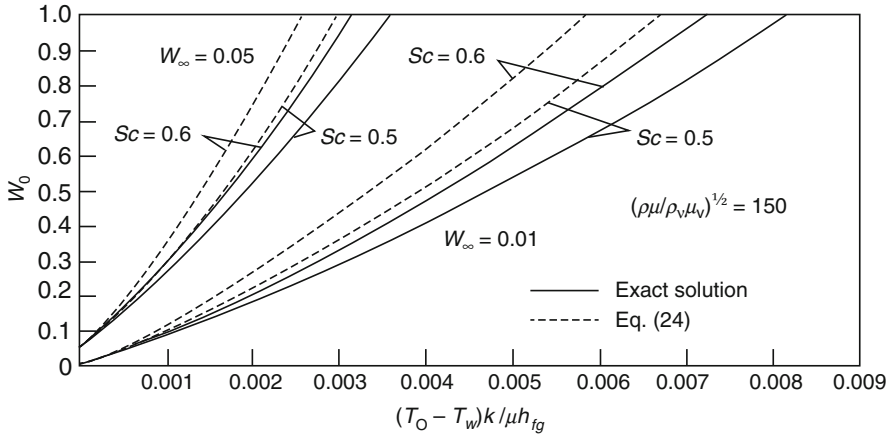

Fig. 3 Comparison of Eq. 24 with exact uniform property solution of Sparrow and Lin (1964) (Reproduced from Rose 1969)

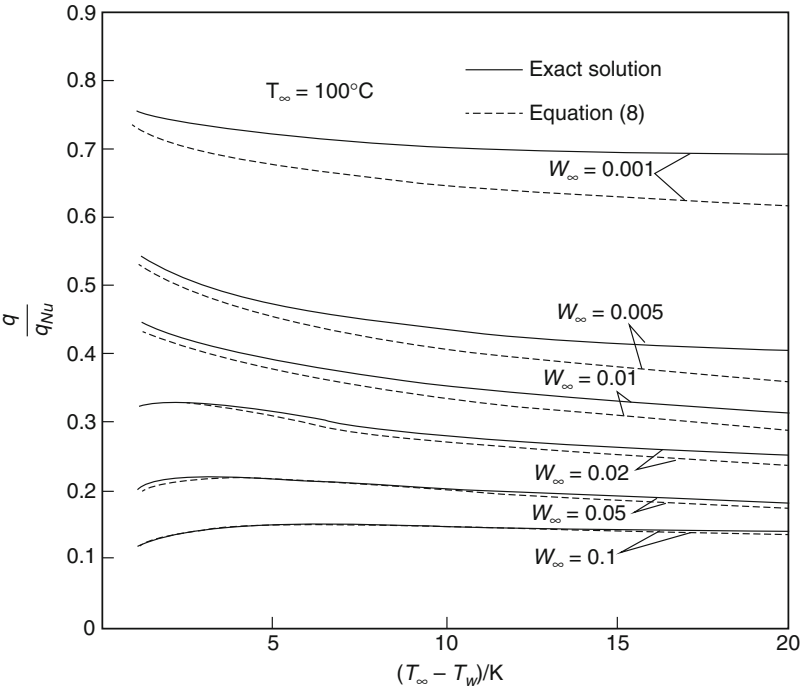

Fig. 4 Comparison of results for steam-air mixtures given by Eq. 24 (and the Nusselt result for the condensate film) with exact variable property solution of Minkowycz and Sparrow (1966) (Reproduced from Rose 1969)

$$\omega = \left\{1 + \beta_x Sc\left(1 + 0.941\beta_x^{1.41} Sc^{0.93}\right)/\zeta\right\}^{-1} \tag{28}$$

where

$$\omega = W_\infty / W_0 \tag{29}$$

$$\beta_x = (m_x/\rho_v U_\infty) Re_x^{1/2} \tag{30}$$

$$\zeta = Sc^{1/2}\left(27.8 + 75.9Sc^{0.306} + 657Sc\right)^{-1/6} \tag{31}$$

Equation 28 is in virtually perfect agreement with the numerical results of Sparrow et al. (1967) for Schmidt number 0.55 and with those of Fujii et al. (1977) for Schmidt numbers 0.2, 0.5, 1.0, and 1.5 and has the advantage that numerical solutions of differential equations are not needed and the result is valid for any vapor-gas combination. For given bulk vapor composition and velocity, Eq. 28 relates the local condensation mass flux m_x and the interface vapor composition W_0. The interface equilibrium condition Eq. 27 relates the interface

temperature T_0 and composition W_0, and Eq. 11 with given T_w, and $q_x = m_x\, h_{fg}$, relates m_x and T_0. Iterative solution of the three simultaneous algebraic equations incorporating appropriate mean property values gives W_0, T_0, and m_x and hence the heat flux q_x, for given values of W_∞, T_w, and u_∞.

For forced convection condensation on a horizontal tube in the presence of a noncondensing gas, Rose (1980), using additional approximations, obtained an algebraic equation based on results for the corresponding problem of heat-transfer with surface suction which may be expressed:

$$\frac{m\,d}{\rho_v D} Re_d^{-1/2} = \left\{ \left[1 + 2.28\, Sc^{1/3} \left(\omega^{-1} - 1 \right) \right]^{1/2} - 1 \right\} / 2 \tag{32}$$

Equation 32, applicable to any vapor-gas mixture, relates condensation mass flux to the bulk and interface composition (and hence temperature) and the vapor velocity. Very close agreement is found with a correlation due to Berman (1969) for steam-air mixtures. As in the flat plate case, Eq. 32 may be solved iteratively with Eq. 27 and an equation such as (Eq. 22) for the condensate film to obtain the heat flux for given tube surface temperature and bulk vapor velocity and composition. The results agreed very well with measurements for steam-air by Mills et al. (1974) as found by Rose (1980) who used Eq. 21 for the condensate film.

4 Film Condensation on Low Integral-Finned Tubes

Low integral-finned tubes such as that shown in Fig. 5 are widely used in refrigeration plant condensers and are known to give large heat-transfer enhancement, typically up to factors around 7 in the effective condensing-side heat-transfer coefficient. This significantly exceeds that expected on the basis of increased area. An early and widely used theoretical result (Beatty and Katz 1948) is based on the Nusselt theory and does not include surface tension effects now known to be of crucial importance. That the Beatty and Katz model appeared satisfactory in many cases is due to the fact surface tension has both beneficial and detrimental effects on heat-transfer which tend to cancel. However, the model predicts that the heat-transfer coefficient continually increases with increasing fin density and conflicts with measurements which indicate optimum values of fin density.

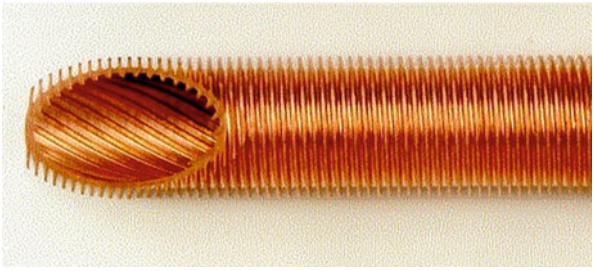

Fig. 5 Tube with low external integral fins (Courtesy Weiland-Werke)

Surface tension gives rise to retention of condensate between the fins (see Fig. 6) which render parts of the fin flanks and interfin tube surface essentially adiabatic. The level of the retained condensate depends on the fin density and is obtained by a balance of capillary and gravity forces. For trapezoidal fins:

$$\phi = \cos^{-1}\{(4\sigma \cos\beta/\rho g b d_o) - 1\} \tag{33}$$

where ϕ is referred to as the retention angle measured from the top of the tube to the level of retained condensate (Honda et al. 1983) and β is the half angle at the fin tip. Note that large values of ϕ correspond to low levels of retention or "flooding." Equation 33 was also obtained as a special case in a more general treatment by Masuda and Rose (1987) who showed that liquid is also retained in the form of wedges at the fin toots on the upper unflooded parts of the tube.

Varying curvature of the condensate film surface along the unflooded parts of the fin results in radial pressure gradients due to varying pressure change across the

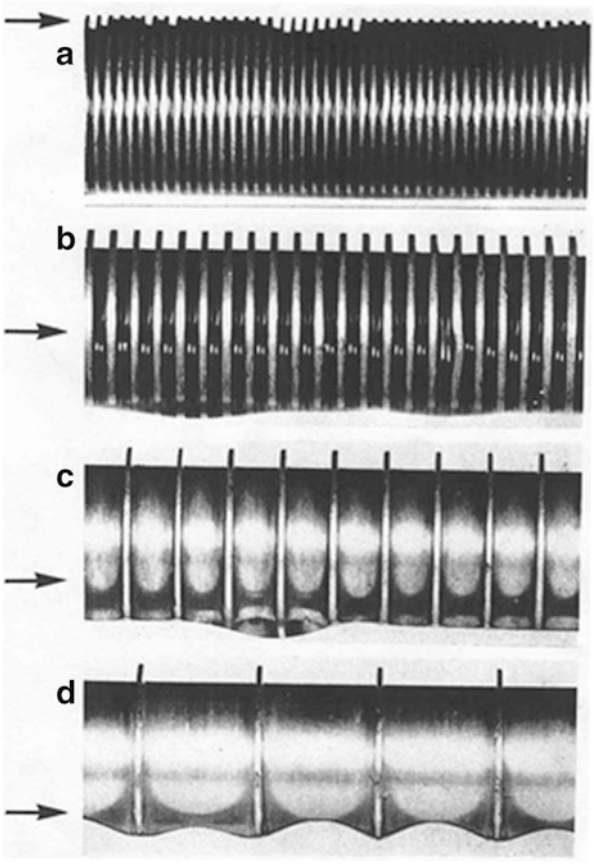

Fig. 6 Condensate retention between fins with different fin densities. The arrow denotes the level of retained liquid (ethylene glycol) (Reproduced from Masuda and Rose 1987)

interface. This leads to local thinning of the condensate film and consequent heat-transfer enhancement. Thus the presence of fins affects the heat-transfer in three ways: (1) increase in surface area which enhances the heat-transfer, (2) capillary retention of condensate between fins which adversely affects heat-transfer, and (3) surface tension-induced pressure gradients which lead to thinner condensate films on parts of the surface and thus enhance heat-transfer.

Involvement of surface curvature and pressure gradients which are not aligned with gravity leads to difficulties in analysis of the heat-transfer problem. Attempted solutions have required significant approximations. Either gravity has been neglected when considering the surface tension-driven radially inward flow of condensate on the fin flank, or only the radial component of the gravity force is included. In some cases (e.g., Karkhu and Borovkov 1971; Rifert 1980; Webb et al. 1985; Adamek and Webb 1990), the problem has been greatly simplified by assuming uniform radial pressure gradient along the fin flank together with assumed radius of curvature of the condensate film surface at the tip and root of the fin. A treatment by Honda and Nozu (1987) showed this approximation to be invalid. Rose (1994) combined the Nusselt theory for the gravity-driven flows and a dimensional analysis approach for those driven by surface tension to obtain, for trapezoidal section fins, an algebraic result with two unknown contents determined by fitting accurate experimental data. The final result is expressed in the form of an *enhancement ratio*, i.e., the heat flux or heat-transfer coefficient for the finned tube divided by the heat flux or heat-transfer coefficient for the smooth tube with the same vapor-surface temperature difference:

$$\varepsilon_{\Delta T} = \frac{d_0}{d_r}\frac{t}{(b+t)}T_t + \frac{\phi}{\pi}\frac{(1-f_f)}{\cos\beta}\left(\frac{d_o^2 - d_r^2}{2d_r(b+t)}\right)T_f + 2.96\frac{\phi}{\pi}(1-f_s)\frac{s}{(b+t)}T_s \tag{34}$$

where

$$f_f = \frac{1-\tan(\beta/2)}{1+\tan(\beta/2)}\cdot\frac{2\sigma\cos\beta}{\rho g d_r h}\cdot\frac{\tan(\phi/2)}{\phi} \tag{35}$$

$$f_s = \frac{1-\tan(\beta/2)}{1+\tan(\beta/2)}\cdot\frac{4\sigma}{\rho g d_r s}\cdot\frac{\tan(\phi/2)}{\phi} \tag{36}$$

$$T_t = \left\{\frac{d_r}{d_o} + 0.509\frac{\sigma d_r}{\widetilde{\rho} g t^3}\right\}^{1/4} \tag{37}$$

$$T_f = \left\{2.815\,\frac{d_r}{h_v} + 0.509\frac{\sigma d_r}{\widetilde{\rho} g h^3}\right\}^{1/4} \tag{38}$$

$$T_s = \left\{3.56\{\xi(\phi)\}^3 + 0.509\frac{\sigma d_r}{\widetilde{\rho} g s^3}\right\}^{1/4} \tag{39}$$

$$h_v = h\phi / \sin\phi \quad \text{for} \quad \phi \leq \pi/2 \tag{40}$$

$$h_v = h\phi/(2 - \sin\phi) \quad \text{for} \quad \phi \geq \pi/2 \tag{41}$$

$$\begin{aligned}\xi(\theta) = & \frac{1}{2^{1/3}\theta^{4/3}}\left[\int_0^\theta \left\{\frac{\int_0^\theta (\sin\theta)^{1/3} d\theta}{(\sin\theta)^{4/3}}\right\}^{-1/4} d\theta\right]^{4/3} \\ & \approx 0.874 + 0.1991 \times 10^{-2}\theta - 0.2642 \times 10^{-1}\theta^2 \\ & + 0.553 \times 10^{-2}\theta^3 - 0.1363 \times 10^{-2}\theta^4\end{aligned} \tag{42}$$

Note that Eq. 34 gives the ratio of heat-transfer coefficient for the finned tube compared with that of a smooth tube with the diameter equal to that *at the fin root*. To obtain the ratio of heat-transfer coefficient for the finned compared with that of a smooth tube with the diameter equal to that *at the fin tip*, the enhancement ratio given by Eq. 34 should be multiplied by $(d_r/d_o)^{3/4}$. Equation 34, which involves only geometric variables, the surface tension and density of the fluid and the specific force of gravity, can be readily used to optimize fin dimensions for maximum enhancement ratio. Comparisons with experimental data are given in Figs. 7, 8, 9, and 10 which demonstrate overall agreement with experiment and the correct dependence on fluid properties and individual fin dimensions when each of the others is held constant. The peak seen in Fig. 8 highlights the importance of fin density, particularly for the case of the refrigerant. The slope discontinuities in Figs. 8 and 9 occur at fin densities and fin heights, respectively, where $\phi = 0$, i.e., the interfin space becomes fully flooded.

In the derivation of Eq. 34, the temperatures of all surfaces of the fin were taken as that at the root of the fin, i.e., neglecting conduction resistance of the fin. This is valid for the case of refrigerants condensing on copper or brass tubes when $\alpha\, h^2/t\, k_w$ is

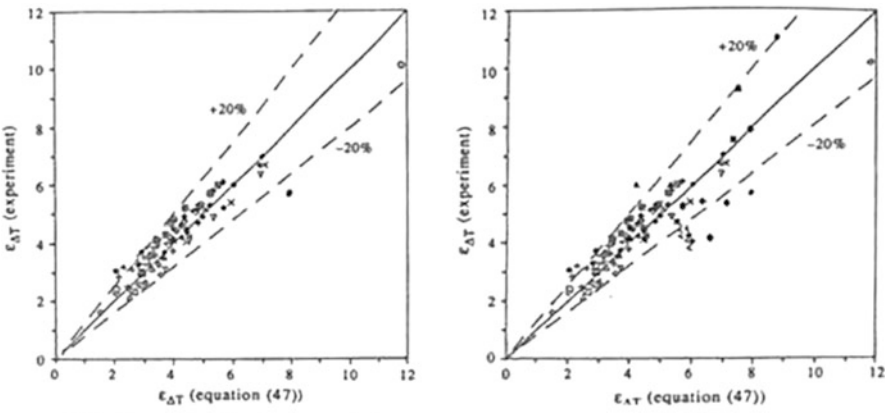

Fig. 7 Comparison of Eq. 34 with experimental data. Measured versus calculated enhancement ratio for various fluids (Symbols are identified in Rose 1994)

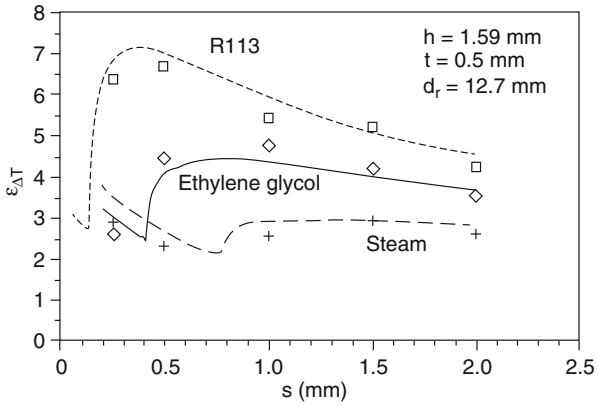

Fig. 8 Comparison of Eq. 34 with experimental data. Dependence of enhancement ratio on space between adjacent fins (Rose 1994)

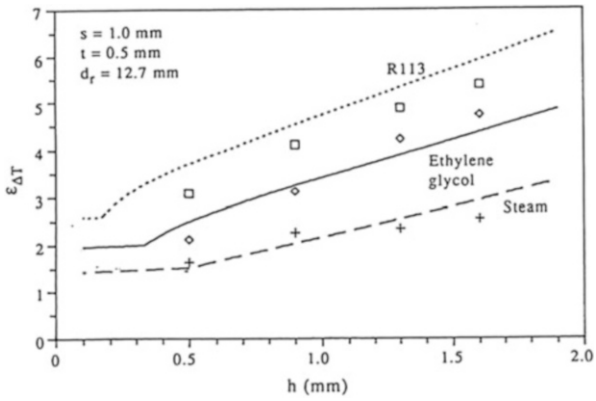

Fig. 9 Comparison of Eq. 34 with experimental data. Dependence of enhancement ratio on height of fins (Rose 1994)

small. A modification of the above result to include fin efficiency has been given by Briggs and Rose (1994). This results in a pair of algebraic simultaneous equations which need to be solved by iteration. For refrigerants condensing on copper or brass tubes, the effect of including fin efficiency is probably less than the accuracy of results predicted by Eq. 34. For condensation of steam on low-conductivity tubes such as stainless steel or titanium, fin efficiency is more important.

It was demonstrated by Briggs and Rose (1998) that significant dependence of enhancement ratio on pressure for steam (decrease from a value of around 3 at 100 kPa to around 2.3 at 10 kPa observed by Wanniarachchi et al. 1985) could be explained on the basis of interface resistance. This is due to the relatively high thermal conductivity of water and very high heat fluxes where the condensate film is extremely thin. For low-conductivity refrigerants, the effect is negligible.

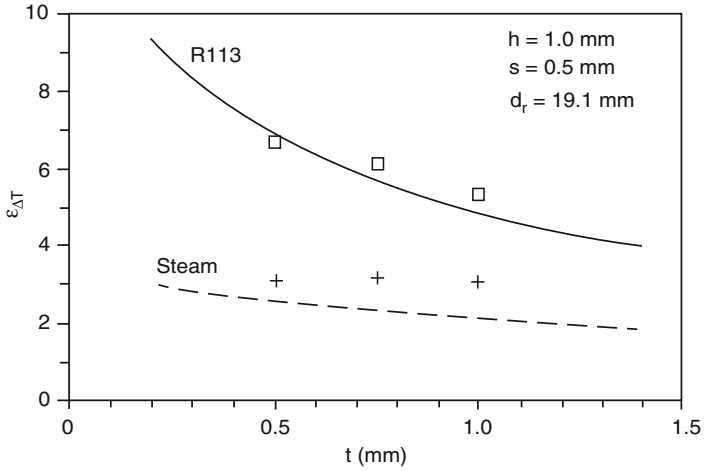

Fig. 10 Comparison of Eq. 34 with experimental data. Dependence of enhancement ratio on thickness of fins (from Rose 1994)

5 Condensation in Microchannels

Tubes with parallel channels with typical dimensions around 1 mm have been found effective in condensation, especially in refrigeration/air-conditioning applications. This is primarily due to surface tension effects. Correlations of experimental data for condensation in microchannels (some of which do not include surface tension) give the vapor-side heat-transfer coefficient as a function of quality and vapor mass flux and not separately dependent on vapor-surface temperature difference and its distribution along the channel. For R134a different correlations based on data for this fluid agree quite well with each other but disagree widely when used for fluids with significantly different properties (see Su et al. 2009). Annular flow occurs at the onset of condensation and might be expected to persist, while the quality remains relatively high. Annular flow has been reported to be the most prevalent mode of condensation by Kim et al. (2012). The case of laminar annular flow, including the effect of surface tension which causes transverse flow of condensate toward the corners, is amenable to analysis.

The theory of laminar annular flow condensation in rectangular and triangular section microchannels (Wang and Rose 2005, 2011) is based only on the approximations of Nusselt (1916) and has no empirical input. Account is taken of transverse surface tension-driven flow of condensate toward the corners, vapor shear stress-driven streamwise flow, and gravity. The Nusselt approach leads to the following differential equation for the local (transverse and streamwise) condensate film thickness:

$$\frac{(\rho-\rho_v)g\cos\beta}{3\nu}\frac{\partial}{\partial x}\left(\delta^3\sin\psi\right)+\frac{\sigma}{3\nu}\frac{\partial}{\partial x}\left\{\delta^3\frac{\partial}{\partial x}\left(\frac{1}{r_c}\right)\right\}+\frac{1}{2\nu}\frac{\partial\left(\tau_i\delta^2\right)}{\partial z}$$
$$-\frac{(\rho-\rho_v)g\sin\beta}{3\nu}\frac{\partial}{\partial z}\left(\delta^3\right)-\frac{1}{3\nu}\frac{\partial}{\partial z}\left(\delta^3\frac{\mathrm{d}P_v}{\mathrm{d}z}\right)=\frac{1}{(1+\zeta\lambda/\delta)}\frac{\lambda(T_v-T_w)}{h_{fg}\delta} \tag{43}$$

where

$$\frac{1}{r_c}=\frac{\partial^2\delta/\partial x^2}{\left\{1+(\partial\delta/\partial x)^2\right\}^{3/2}} \tag{44}$$

and

$$\zeta=\frac{(\gamma+1)}{4\xi(\gamma-1)}v_{fg}T_v(RT_v)^{1/2}/{h_{fg}}^2 \tag{45}$$

and x and z are the transverse and streamwise coordinates, respectively. The corresponding polar coordinate equation used to treat the corners is given by Wang and Rose (2005) for a horizontal channel and by Wang and Rose (2011) when including channel inclination.

Given the necessary boundary conditions, Eq. 43, together with its polar counterpart, can be solved numerically to give local condensate film thickness and hence local (averaged around the channel perimeter, p) heat-transfer coefficient. Local quality, given by

$$\chi=1-\frac{\rho}{AG}\int_0^p\left(\int_0^\delta u\,dy\right)dx \tag{46}$$

where y is the coordinate normal to the channel surface, may also be obtained. Four boundary conditions are required for the transverse direction. (Note that the curvature expression Eq. 44 has a second derivative and the curvature term in Eq. 43 is twice differentiated.) For channel sections with a vertical axis of symmetry, these are provided by the fact that the first and third derivatives are zero at the central top and bottom positions of the channel cross section. For cases where the vapor is saturated or superheated at inlet, the required streamwise boundary condition is provided by the fact that the condensate film thickness is zero over the channel perimeter at the position of onset of condensation. Most experiments have been done with quality less the one at inlet, and correlations for the heat-transfer coefficient are given in terms of vapor quality and mass flux, irrespective of vapor-surface temperature difference and position along the channel. For these cases, there is no streamwise boundary condition, and only approximate comparisons with the laminar annular flow model can be made.

Solutions of Eq. 43 for cases where the vapor is saturated at inlet indicate that, while the variation of heat-transfer coefficient along the channel depends strongly on temperature difference, the dependence is much weaker when heat-transfer

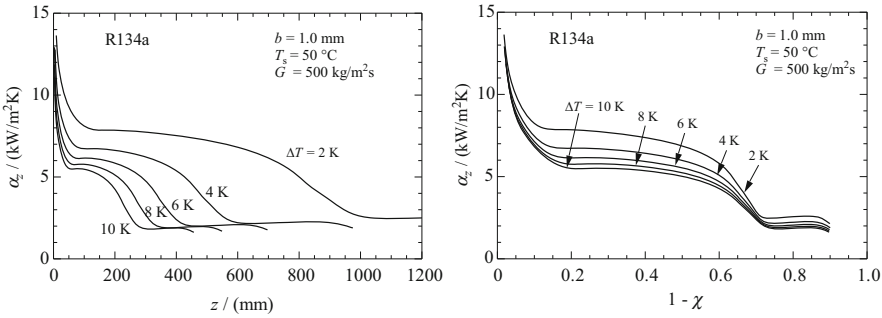

Fig. 11 Dependence of heat-transfer coefficient on distance along channel and quality (Wang and Rose 2011)

coefficient is plotted against quality (as given by Eq. 46) as shown in Fig. 11 and probably within experimental uncertainty.

Approximate comparisons of correlations with theory may be made by taking, in the solutions, saturated vapor at inlet and a typical vapor-surface temperature difference (taken to be uniform along the channel) and plotting heat-transfer coefficient against quality. These show generally good agreement (see Fig. 12). In this approximate method of comparison, the theory overestimates the heat-transfer coefficient at low vapor mass flux and relatively high quality and slightly underestimates at high vapor mass flux.

In two investigations (Koyama et al. 2003a, b; Kim and Mudawar 2012; Kim et al. 2012), where the vapor was superheated at inlet and the vapor-surface temperature difference along the channel was obtained, direct comparison with theory can be made. These are shown in Figs. 13, 14, and 15. Notwithstanding the fact that in the case of Kim and co-workers, condensation did not occur on the upper transparent surface in the experiments, the agreement for wide ranges of vapor mass flux and quality is remarkable when noting that the theory has no empirical input.

6 Dropwise Condensation

6.1 Experimental Investigations

The topic of dropwise condensation has been extensively investigated since Schmidt et al. (1936) drew attention to this second ideal mode of condensation which occurs on macroscopically uniformly hydrophobic surfaces with heat-transfer coefficients significantly higher than for film condensation. In early experimental studies, the condensing surface was treated with a non-wetting agent such as oleic acid to promote dropwise condensation. The *promoter* is thought to bond with copper or copper-containing surfaces and excess promoter removed during condensation to leave a monomolecular layer with negligible thermal resistance. Subsequently

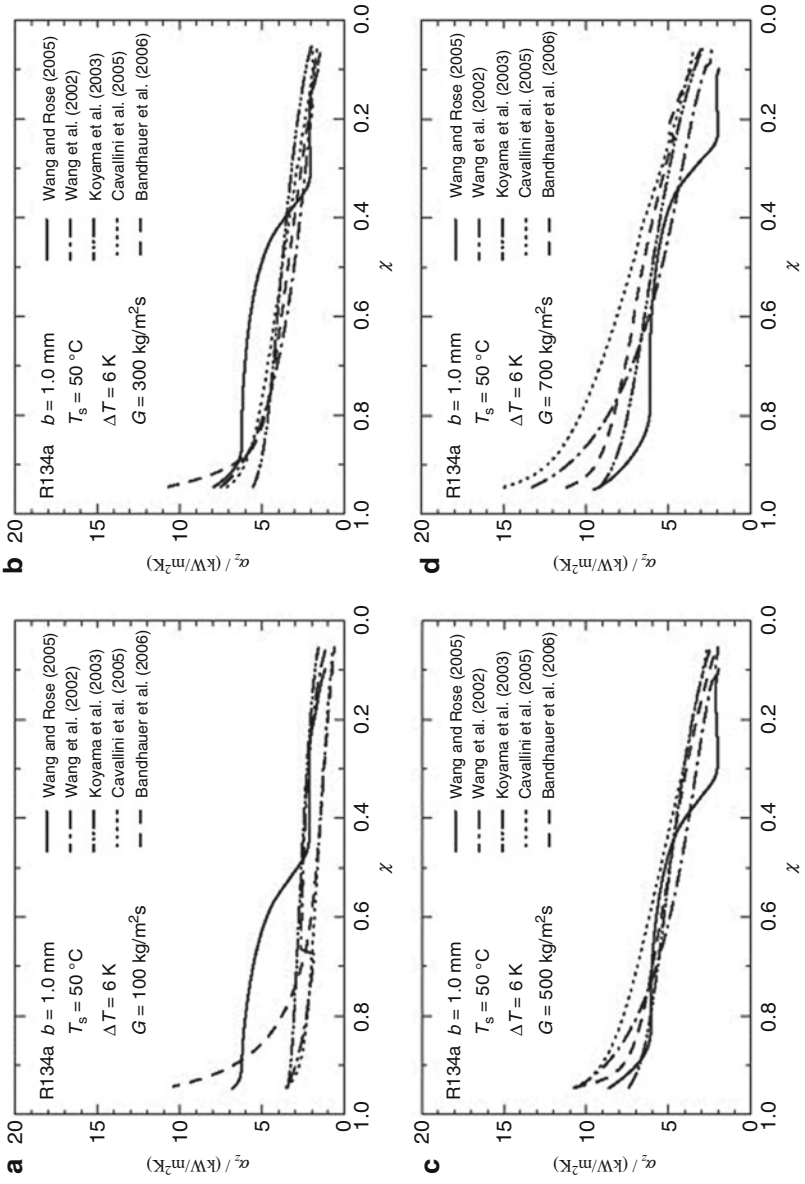

Fig. 12 Approximate comparison between theory and correlations for condensation of R134a in square microchannels (Su et al. 2009)

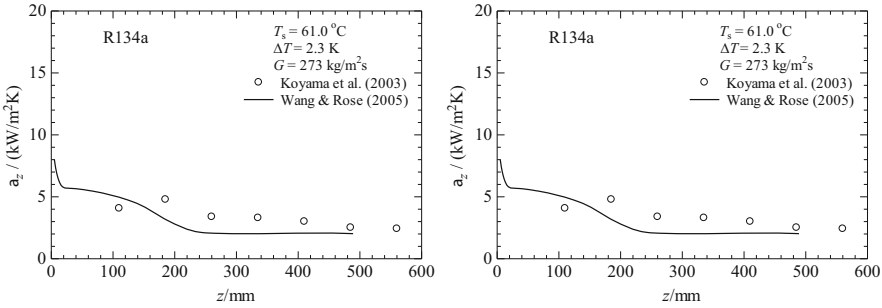

Fig. 13 Comparison of theory and experimental data of Koyama et al. (2003a, b) for R134a. Heat-transfer coefficient versus distance along channel from position of onset of condensation

potential promoters were investigated with the aim of producing durable dropwise condensation. Promoters comprising molecules which would bond more strongly with the metal were synthesized in the 1950s. When using a promoter of this kind in heat-transfer measurements, it was found that the heat-transfer coefficient increased markedly (by around 50%) during around 4 h from the commencement of tests (Le Fevre and Rose 1965; Citakoglu and Rose 1968). This was attributed to removal of excess promoter.

As discussed by Rose (1964), durability trials of some of the synthetic promoters showed no evidence of breakdown in tests lasting up to 3,530 h under laboratory conditions. Tests on marine and power station condensers indicated lifetimes of 5 months to a year or more.

The traditional promoters described above all exhibited contact angle near to 90°, i.e., approximately hemispherical drops. Most recently, investigations of dropwise condensation on "nanostructured" surfaces show apparent contact angles significantly higher than 90° and drops which, under some circumstances, spring spontaneously away from the surface (see, for instance, Enright et al. 2014; Miljkovic et al. 2016). To date such surfaces have not demonstrated superior heat-transfer performance or durability.

Figure 16 shows photographs of *ideal* dropwise condensation of steam. The moving droplets fall vertically with high acceleration. Their speed is such that for the higher heat flux case, and when viewed in real time, they cannot be clearly distinguished, and the surface appears blurred.

During dropwise condensation, the vapor-surface temperature difference is small and susceptible to error caused by the presence of even minute amounts of air in the steam. Many experimental investigations have been vitiated by the presence of air in the steam, and the accuracy of surface temperature measurements was often inadequate. While all experimental investigations reported significant enhancement over film condensation, there are wide disagreements between different investigations as shown in Fig. 17.

A key point, now well established and first reported by Wenzel (1957), is that, in contrast to film condensation, the heat-transfer coefficient *increases* with increasing

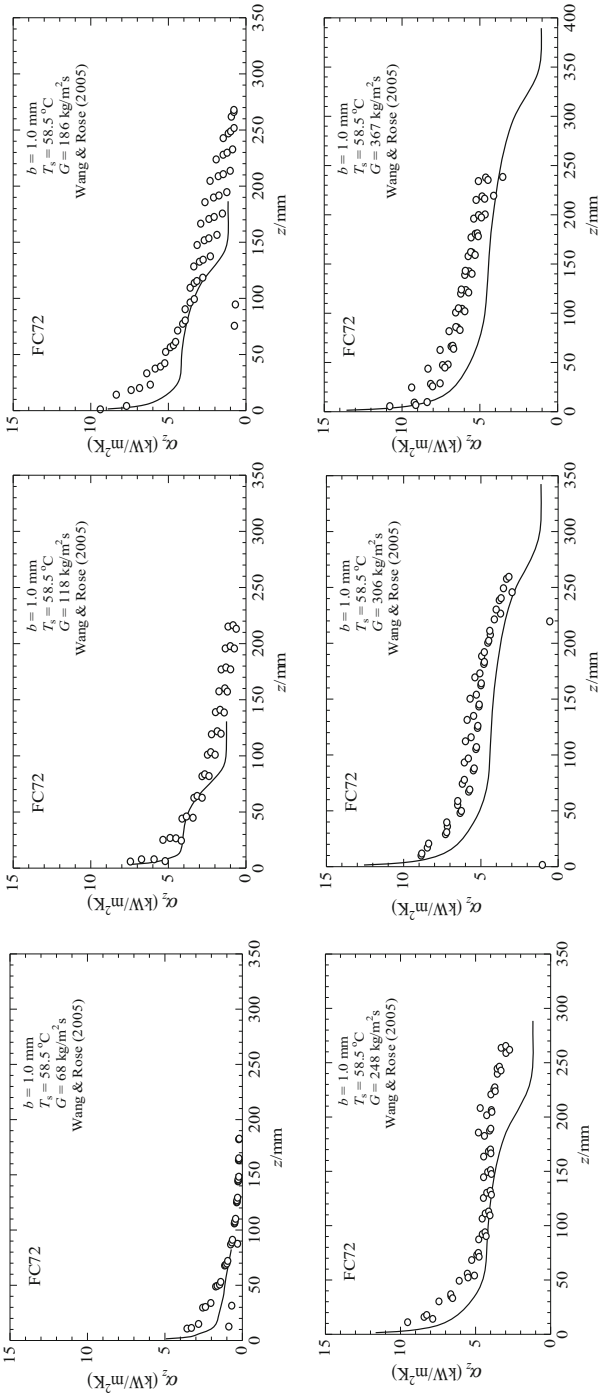

Fig. 14 Comparison of theory and experimental data of Kim and Mudawar (2012) and Kim et al. (2012) for FC72. Heat-transfer coefficient versus distance along the channel from position of onset of condensation (The author is grateful to Professors Mudawar and Kim for providing details of their experimental data)

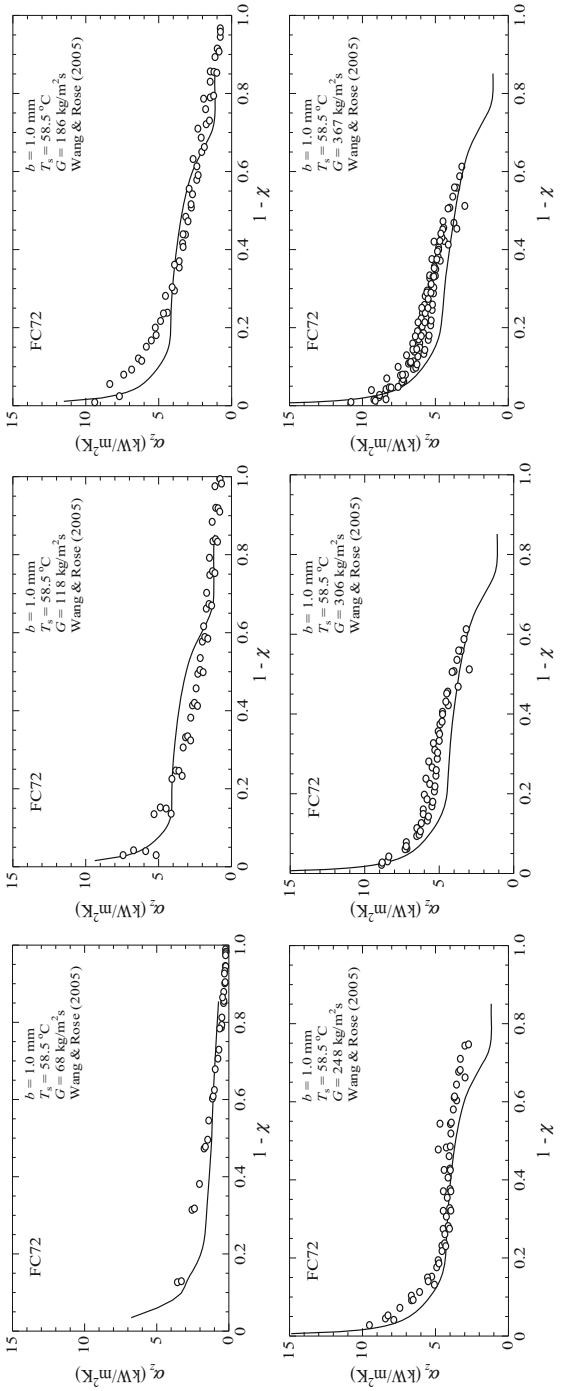

Fig. 15 Comparison of theory and experimental data of Kim and Mudawar (2012) and Kim et al. (2012) for FC72. Heat-transfer coefficient versus quality (The author is grateful to Professors Mudawar and Kim for providing details of their experimental data)

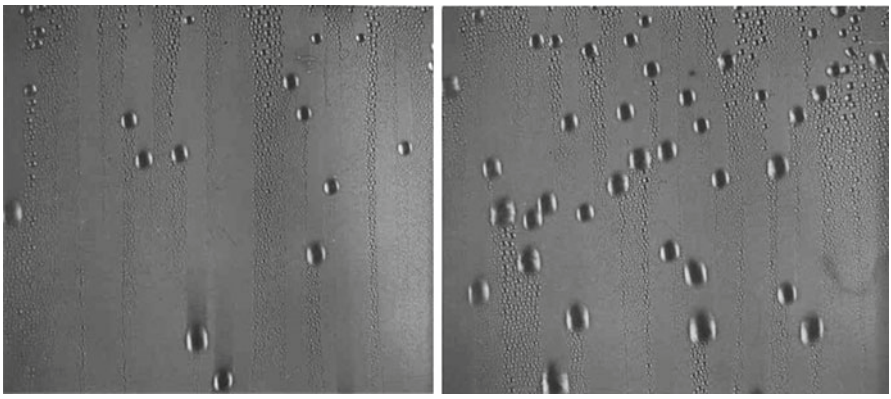

Heat flux 0.4 MW/m^2; $\Delta T = 2$ K;
Heat-transfer coefficient 0.2 MW/m^2 K

Heat flux 1.4 MW/m^2; $\Delta T = 4$ K;
Heat-transfer coefficient 0.35 MW/m^2 K

Fig. 16 Dropwise condensation of steam at near-atmospheric pressure on a vertical plane copper surface (5 × 5 cm) promoted with dioctadecyl disulfide (Rose 1964)

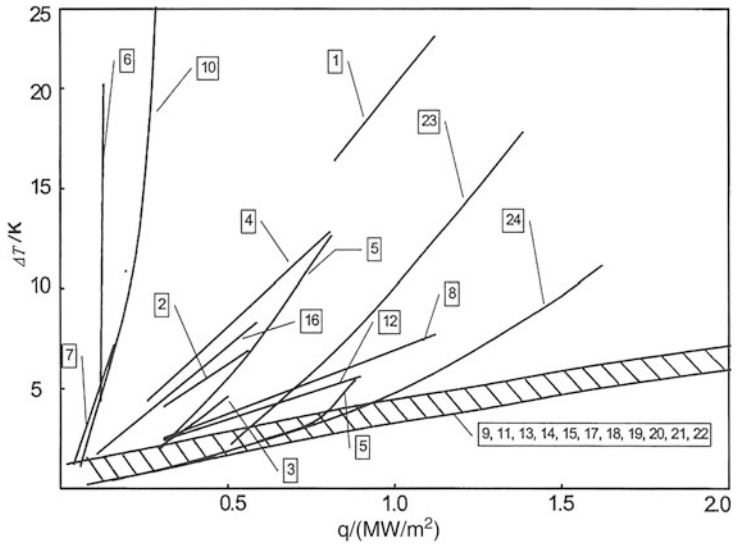

Fig. 17 Heat-transfer data for dropwise condensation of steam at near-atmospheric pressure (Sources are identified in Rose 2002)

vapor-surface temperature difference (and hence with increasing heat flux) as shown in Fig. 18.

Data for which effects of noncondensing gases were eliminated and the surface temperature was measured with sufficiently high accuracy are those in the

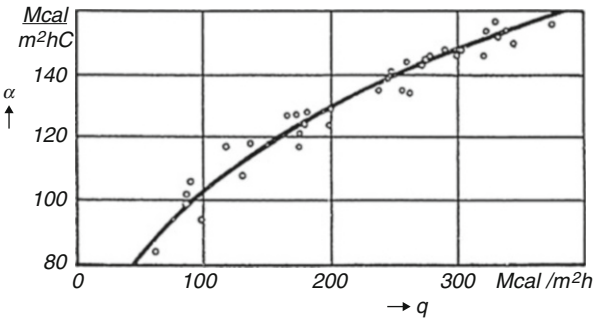

Fig. 18 Dropwise condensation of steam at near-atmospheric pressure on a vertical plane copper surface. Heat-transfer coefficient versus heat flux (Wenzel 1957)

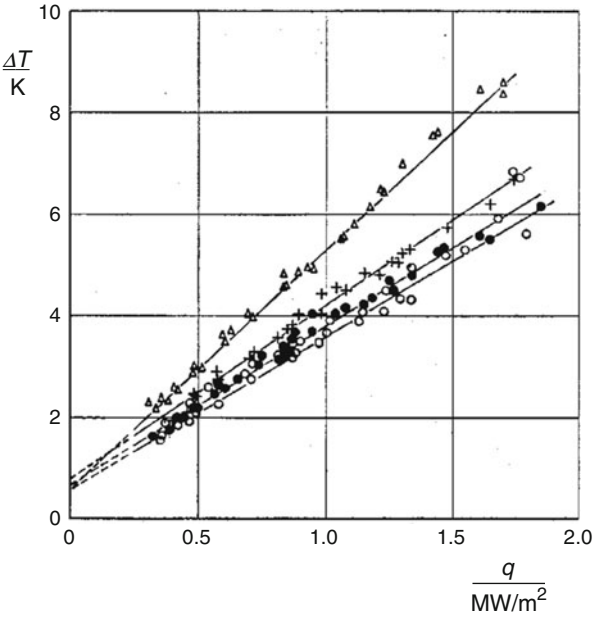

Fig. 19 Vapor-surface temperature difference versus heat flux for four promoters (Le Fevre and Rose 1964, 1965)

shaded band in Fig. 17 with the highest heat-transfer coefficients. Figure 19 shows results for which extreme care was taken to measure the surface temperature accurately and to avoid effects of noncondensing gases. Tests were repeated on three separate days for each of four promoters, dioctadecyl disulfide [$C_{18}H_{37}SSC_{18}H_{37}$], octadecylamine [$C_{18}H_{37}NH_2$], Di-S-octadecyl 00-1, 10-decanedixanthate [$C_{18}H_{37}SSCO(CH_2)_{10}OCSSC_{18}H_{37}$], and dodecanetris (ethanethio) silane [$C_{12}H_{25}Si(SC_2H_5)_3$], and show clear differences between results for the different promoters.

For condensation of steam at atmospheric pressure, heat-transfer coefficients are around 20 times those for film condensation. Accurate measurements at lower pressures (Wilmshurst and Rose 1970) show that the heat-transfer

coefficient decreases with decreasing pressure. At power station condenser pressures, the heat-transfer coefficient exceeds that for film condensation by a factor of around 10.

6.2 Theory of Dropwise Condensation

6.2.1 Introduction

Dropwise condensation is a cyclic phenomenon in which primary drops form at nucleation sites exposed by sweeping of the surface by falling drops. The primary drops grow by condensation and coalescence with neighboring drops, and new primary drops nucleate on the exposed surface until the region is swept again by a falling drop. The primary drops are closely packed with nucleation site densities exceeding 10^{10} per cm^2 (Tanasawa et al. 1974). Many thousands of coalescences take place in the formation of the largest drops. The process is described in detail by Rose and Glicksman (1973). A quasi-steady approach was used in the theory of Le Fevre and Rose (1966) in which the heat-transfer through a drop of given size is combined with an expression for the mean distribution of drop sizes to obtain the surface heat flux for a given vapor-surface temperature difference. Drops range in size from the smallest on which condensation can take place at nucleation sites to the largest to which drops grow before the region is swept by a falling drop. The drops range in size from nanometer to millimeter scale. Condensation on the smallest drops is inhibited by the surface curvature effect which necessitates cooling of the vapor below its normal saturation temperature. Those drops somewhat larger than primary drops, where the curvature effect becomes less significant, experience intense condensation rates, and the temperature drop at the vapor-condensate interface is important. For the largest drops, the dominant thermal resistance is that due to conduction. Owing to the range of drop sizes, it is necessary that all three effects are included. Since the sliding drops grow as they descend by sweeping the stationary drops in their path, lower parts of the surface are swept more frequently, and all sliding drops start from a region very near to the top of the surface (Rose 1976). Except at very high condensation rates (heat flux 2–3 MW/m^2), the sliding drops do not occupy an appreciable proportion of the surface (Rose 1967).

6.2.2 Heat-Transfer Through a Drop of Given Size

Conduction in a Drop

The curved surface and base of a drop both have nonuniform temperatures which are equal at the perimeter of the base. An early graphical solution of the conduction problem by Fatica and Katz (1949), and subsequently by others, uses uniform temperatures over the curved and plane surfaces of a drop. In this case, the temperature discontinuity at the edge of the base results in infinite heat-transfer. Purported solutions are grid dependent. When the interface temperature drop is included, valid numerical solutions may be obtained (Umur and Griffith 1965). In order to simplify

the problem, an effective average temperature drop between the curved and plane surfaces given by

$$\Delta T_c = K_1 r q_b / \lambda \tag{47}$$

is adopted in the theory of Le Fevre and Rose (1966) where K_1 is a constant of order of magnitude unity, r is the base radius of the drop, q_b is the mean heat flux at the base of the drop, and λ is the thermal conductivity of the drop. For a hemispherical drop modeled as a right circular cylinder with adiabatic sides and the same base radius and volume as the drop, K_1 would be 2/3.

Surface Curvature Effect

As well as playing a vital role in the process of nucleation by determining the size of the smallest viable drop, surface curvature introduces an effective resistance to heat-transfer which is significant for the very small drops. The continuity of Gibbs function together with the pressure difference due to surface tension across the curved interface requires a temperature difference ΔT_σ, between the vapor adjacent to the liquid surface and the normal saturation temperature given by

$$\Delta T_\sigma = \frac{2\sigma T_{sat}}{r_c \rho h_{fg}} \tag{48}$$

where σ is surface tension, T_{sat} is the vapor saturation temperature, ρ is condensate density, h_{fg} is specific latent heat of vaporization, and r_c is the radius of curvature of the liquid surface. If the drop is a segment of a sphere

$$r = r_c \sin\beta \tag{49}$$

where β is the contact angle. In order that condensation may occur, the vapor adjacent to the drop surface must be subcooled below its normal saturation temperature by an amount ΔT_σ.

Interface Temperature Drop

From Eq. 3, the interface temperature drop at the curved interface is given by

$$\Delta T_i = 3 q_i v_{fg} T_{sat} (R T_{sat})^{1/2} (\gamma + 1)/8(\gamma - 1) {h_{fg}}^2 \tag{50}$$

where q_i is the heat flux at the vapor-liquid interface and v_{fg} is the difference between the vapor and liquid specific volumes. When calculating the heat flux for the whole surface, it is necessary to express the interface temperature difference in terms of the heat flux at the base of the drop q_b by writing

$$q_i = K_{20} q_b \tag{51}$$

where K_{20} is the ratio of the base area to the curved surface area of the drop. For a drop in the form of a spherical segment with contact angle β

$$K_{20} = \frac{1}{2}(1 + \cos\beta) \tag{52}$$

and for hemispherical drops $K_{20} = 0.5$. Equations 50 and 51 give

$$\Delta T_i = 3K_{20} q_b v_{fg} T_{sat} (RT_{sat})^{1/2} (\gamma + 1)/8(\gamma - 1) {h_{fg}}^2 \tag{53}$$

Temperature Drop in Promoter Layer

Small differences in the heat-transfer performance of different promoters (see Fig. 19) suggest that the temperature drop across the promoter layer, perhaps only a few promoter molecules thick (Le Fevre and Rose 1966), may play a significant role. This is due to the intense heat fluxes at the base of very small drops. For promoter layer thickness and thermal conductivity t_p and λ_p, respectively, the temperature drop across the promoter layer under a drop is

$$\Delta T_p = q_b \frac{t_p}{\lambda_p} \tag{54}$$

Heat Flux at the Base of a Drop

Equating the sum of the four temperature differences to the bulk vapor-surface temperature difference ΔT and rearranging gives:

$$q_b = \frac{\Delta T - \dfrac{2\sigma T_{sat} \sin\beta}{r \rho h_{fg}}}{\dfrac{K_1 r}{\lambda} + \dfrac{3K_{20} v_{fg} T_{sat} (RT_{sat})^{1/2} (\gamma + 1)}{8 {h_{fg}}^2 (\gamma - 1)} + \dfrac{t_p}{\lambda_p}} \tag{55}$$

The form Eq. 55 would be strictly correct (without the curvature temperature drop in the numerator) if a drop were modeled as a cylinder with adiabatic sides and the same volume and base radius as the drop. For a hemispherical drop, K_1 would be 2/3 and K_{20} would be 1/2. Equation 55 differs very slightly from that given by Le Fevre and Rose (1966) in that a more up-to-date kinetic theory result has been used here for the interface term and ξ has been taken as 2/3. This minor change has negligible effect on calculated results. Equation 55 has been used, sometimes with small modifications, by several later investigators. A more rigorous derivation of this equation is given in the original paper by Le Fevre and Rose (1966). Equation 55 may be written

$$q_b = \frac{\dfrac{\Delta T}{T_{sat}} - \dfrac{L_0}{r}}{\dfrac{K_1 r}{Q_1 L_0} + \dfrac{K_{20}}{Q_2} + \dfrac{t_p}{T_{sat} \lambda_p}} \tag{56}$$

where

$$L_0 = 2\sigma \sin\beta/\rho h_{fg} \tag{57}$$

is a combination of properties having dimensions of length and

$$Q_1 = \lambda T_{sat} \rho h_{fg}/2\sigma \sin\beta \tag{58}$$

and

$$Q_2 = \frac{8{h_{fg}}^2(\gamma - 1)}{3v_{fg}(RT_{sat})^{1/2}(\gamma + 1)} \tag{59}$$

are combinations of properties having dimensions of heat flux.

Then, introducing a promoter layer-dependent constant defined

$$K_2 = K_{20} + \frac{t_p Q_2}{\lambda_p T_{sat}} \tag{60}$$

Equation 56 may be written

$$q_b = \frac{\dfrac{\Delta T}{T} - \dfrac{L_0}{r}}{\dfrac{K_1 r}{Q_1 L_0} + \dfrac{K_2}{Q_2}} \tag{61}$$

K_2 depends on drop shape (through K_{20}) and properties of the condensing fluid (through Q_2) as well the saturation temperature and promoter layer thickness and conductivity. For specified conditions, say for condensation of steam at atmospheric pressure (Q_{21}, T_{1sat}), the value of K_2 would be

$$K_{21} = K_{20} + \frac{t_p Q_{21}}{\lambda_p T_{1sat}} \tag{62}$$

where Q_{21} is given by Eq. 59 with properties of steam at $T_{sat} = T_{1sat} = 373.15$ K and is equal to 2.556 GW/m^2.

From Eqs. 60 and 62

$$K_2 = K_{20} + (K_{21} - K_{20})\frac{Q_2}{Q_{21}}\frac{T_{1sat}}{T_{sat}} \tag{63}$$

Equation 63 enables K_2 to be calculated from K_{21}; K_{21} depends on the promoter and K_{20} but not on fluid properties. K_2 would be equal to K_{20} if the promoter layer offered no thermal resistance. In their original paper, Le Fevre and Rose (1966) did not presume that the difference in promoter performance was necessarily attributable to conduction

in the promoter layer. This does not invalidate Eqs. 61 and 63. There is evidence (see Rose 1964) however that conduction in the promoter layer may indeed be responsible.

6.2.3 Distribution of Drop Sizes

Drops continue to grow by coalescence and condensation until a region of the surface is swept by a falling droplet. Many thousands of coalescences take place in the formation of the largest drops. Details of the growth and coalescence process have been considered by Tanaka (1975) and others. The success of the theory described here is in part attributable to the decision to disregard detail of the drop growth process and to use a mean effective, steady, size distribution function given by:

$$f\left(\frac{r}{r_{\max}}\right) = 1 - \left(\frac{r}{r_{\max}}\right)^{1/n} \tag{64}$$

where f is the fraction of surface area covered by drops with base radius greater than r, $r_{\max}$ is the effective mean base radius of the largest drops, and n is a constant. For any n, Eq. 64 satisfies the conditions that no area is covered by drops larger than the largest and that as the smallest drop radius approaches zero, the entire surface is covered. A value $n = 3$ was selected by Le Fevre and Rose (1966) based on comparison of the final result with accurate experimental heat-transfer data for dropwise condensation of steam at near-atmospheric pressure. Equation 64 implies

$$A(r)dr = -f'\left(\frac{r}{r_{\max}}\right)\frac{dr}{r_{\max}} = \frac{1}{n\,r_{\max}}\left(\frac{r}{r_{\max}}\right)^{\frac{1}{n}-1} dr \tag{65}$$

where $A(r)\,dr$ is the fraction of surface area covered by drops with base radius in the range r, $r+dr$,
and

$$N(r)dr = \frac{1}{\pi r^2 n\, r_{\max}}\left(\frac{r}{r_{\max}}\right)^{\frac{1}{n}-1} dr \tag{66}$$

where $N(r)dr$ is the number of drops per area with base radius in the range r to $r+dr$. Equation 66, with $n = 3$, later received support from size distribution theory independent of heat-transfer considerations (Rose and Glicksman 1973) and optical measurements (Graham 1969; Tanasawa and Ochiai 1973) as shown in Fig. 20.

6.2.4 Heat Flux for Whole Surface

The heat flux for the whole surface, q, is given

$$q = \int_{r_{\min}}^{r_{\max}} q_b A(r)dr = -\int_{r_{\min}}^{r_{\max}} \frac{q_b}{r_{\max}} f'\left(\frac{r}{r_{\max}}\right) dr \tag{67}$$

where $r_{\min}$ is the base radius of the smallest viable drop given, from Eqs. 48 and 49, by

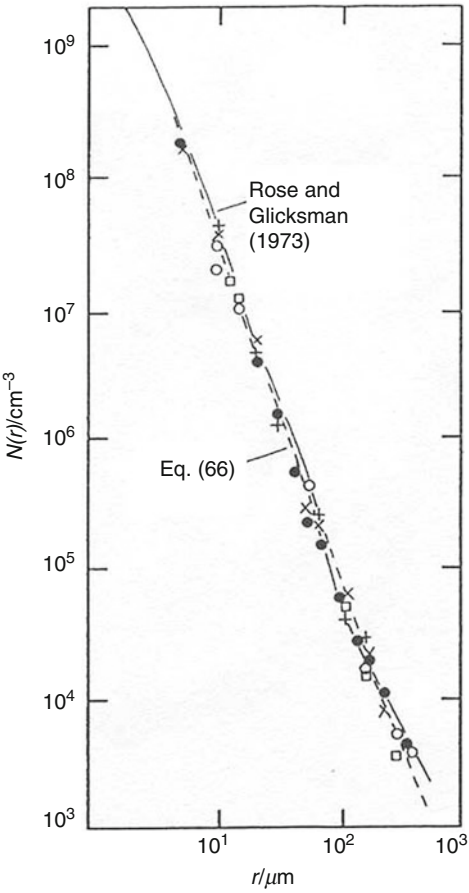

Fig. 20 Comparison of Eq. 66 with $n = 3$ with size distribution model of Rose and Glicksman (1973) and measurements of Graham (1969) and Tanasawa and Ochiai (1973)

$$r_{\min} = \frac{2\sigma T_{sat} \sin\beta}{\rho h_{fg} \Delta T} = \frac{L_0 T_{sat}}{\Delta T} \tag{68}$$

On the basis of dimensional analysis, $r_{\max}$ is taken as

$$r_{\max} = K_3 \left(\frac{\sigma}{g\left(\rho_f - \rho_g\right)} \right)^{1/2} = K_3 L_3 \tag{69}$$

where K_3 is a constant, g is the specific force of gravity, ρ_f and ρ_g are the liquid and vapor densities, respectively, and

$$L_3 = \left(\frac{\sigma}{g\left(\rho_f - \rho_g\right)} \right)^{1/2} \tag{70}$$

is a combination of properties with dimensions of length. The constant K_3 might be estimated from photographs noting that r_{max} is the effective mean radius of the largest drops which is somewhat smaller than the largest visible non-sliding drop (see Rose and Glicksman 1973). A value of r_{max} of 1 mm would give $K_3 = 0.4$.

Equation 67 with Eqs. 65 and 69 leads to

$$q^* = \theta_0^{1/n}\left(\frac{1+\theta}{n}\right)\int_{\theta_0}^{\theta}\frac{z^{-1/n}}{1+z}\,dz - \theta_0^{1/n}\left(\frac{\theta^{1-1/n}-\theta_0^{1-1/n}}{n-1}\right) \tag{71}$$

where

$$q^* = \left(K_2{}^2/K_1\right)\left(Q_1/Q_2{}^2\right)q \tag{72}$$

is dimensionless heat flux,

$$\theta = (K_2/K_1)(Q_1/Q_2)(\Delta T/T_{sat}) \tag{73}$$

is dimensionless temperature difference, and

$$\theta_0 = (K_2/K_1K_3)(Q_1/Q_2)(L_0/L_3) \tag{74}$$

is a dimensionless quantity.

Equation 71 may be written

$$q^*\theta_0{}^{-1/n} = (1+\theta)\left\{I_n\left(\theta^{1/n}\right) - I_n\left(\theta_0{}^{1/n}\right)\right\} - \left(\theta^{1-1/n} - \theta_0{}^{1-1/n}\right)/(n-1) \tag{75}$$

where

$$I_n(z) = (\pi/n)/\sin(\pi/n) - \int_0^{z^{-1}}\frac{dx}{1+x^n} \tag{76}$$

Since in all physically significant cases $\theta_0/\theta << 1$ Eq. 75 simplifies to

$$q^*\theta_0{}^{-1/n} = (1+\theta)I_n\left(\theta^{1/n}\right) - \left(\theta^{1-1/n}\right)/(n-1) \tag{77}$$

Equation 77 gives the relation between the heat flux and vapor-surface temperature difference for drop size distributions of the form given in Eq. 64. Closed form expressions for $I_n(z)$ for various values of n and series solutions for any n are given by Le Fevre and Rose (1966). In particular, for $n = 3$

$$I_3(z) = \frac{1}{\sqrt{3}}\left\{\frac{\pi}{2} - \arctan\left(\frac{2-z}{z\sqrt{3}}\right)\right\} - \frac{1}{6}\ln\left\{\frac{(1+z)^3}{1+z^3}\right\} \tag{78}$$

6.2.5 Values of the Constants and Comparison with Experimental Data

The values $n = 3$, $K_1 = 2/3$, and $K_3 = 0.4$ were assigned by Le Fevre and Rose (1966) by fitting accurate experimental heat-transfer data for dropwise condensation of steam at atmospheric pressure. These are all close to values which might be estimated without reference to heat-transfer data. The heat-transfer data used in determining the constants were for cases where the contact angle was near to 90° (near hemispherical drops). Appropriate values of the constants might be expected to differ for cases where the contact angle is significantly different from 90°. The values obtained for the promoter-dependent constant K_{21} ranged between approximately 0.5 and 2 for eight promoters. Most of the data used to evaluate the constants were for the promoter dioctadecyl disulfide for which K_{21} was found to be 1.01. If promoter resistance is attributed to conduction in the promoter layer, this would indicate negligible layer thickness for a promoter with $K_{21} = 0.5$ and a layer thickness of order 0.1 μm when $K_{21} = 2$ (see Le Fevre and Rose 1966).

Figure 21 compares theoretical results (using the constants given above and $K_{21} = 1.01$) with experimental data for condensation of steam at close to atmospheric pressure. Figure 22 shows comparisons for subsequent data from measurements at lower pressures. Experiment and theory indicate that the heat-transfer coefficient increases with increasing vapor-surface temperature difference and decreases with decreasing pressure. The former is due to the increase in density of active nucleation sites (reflected in the decrease of the lower limit of the integral in Eq. 67 with increasing temperature difference) and the latter to the increasing importance of the interface temperature drop at low vapor pressure (reflected in the increase in v_{fg} in Eq. 55). As

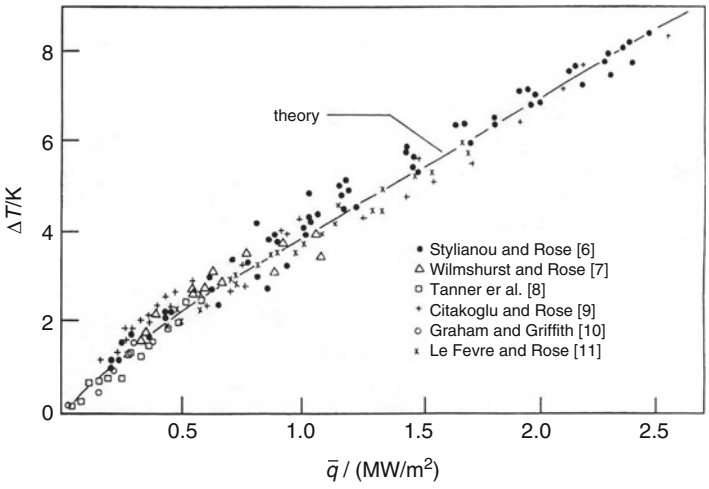

Fig. 21 Comparison of theory with experimental data for dropwise condensation of steam at near-atmospheric pressure (For sources of the data, see Stylianou and Rose 1980)

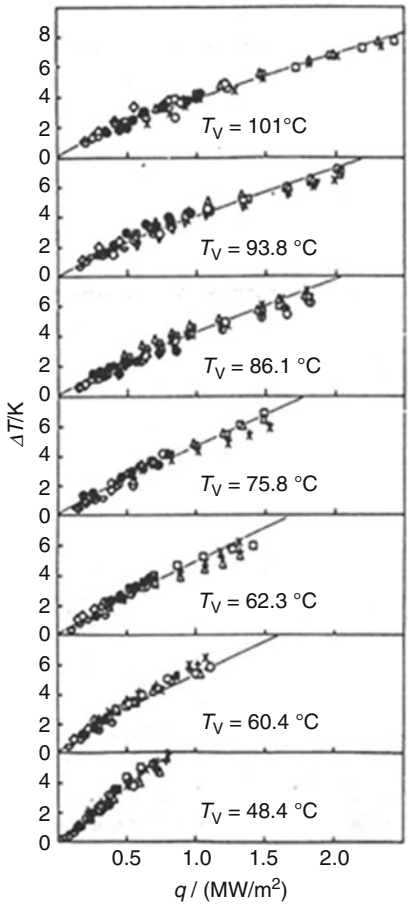

Fig. 22 Comparison with of theory with experimental data of Wilmshurst and Rose (1970) for dropwise condensation of steam at different pressures. T_v is vapor temperature

noted in Rose (2002), for practical purposes, the experimental and theoretical predictions are adequately represented for dropwise condensation of steam by

$$q/\left(\mathrm{kW/m^2}\right) = \theta^{0.8}\left\{5\ (\Delta T/\mathrm{K}) + 0.3\ (\Delta T/\mathrm{K})^2\right\} \tag{79}$$

where θ is Celsius temperature.

Experimental data have been obtained (Tanasawa 1974; Tanasawa et al. 1974) where the size of the largest drops was varied by different means (plate inclination, vapor shear, centrifugal force). For the range of ΔT in these experiments, the heat-transfer coefficient was essentially constant. The theory, using an average of the experimental values of ΔT, is compared with these data in Fig. 23. As may be seen, the heat-transfer coefficient and its dependence on maximum drop size are correctly predicted.

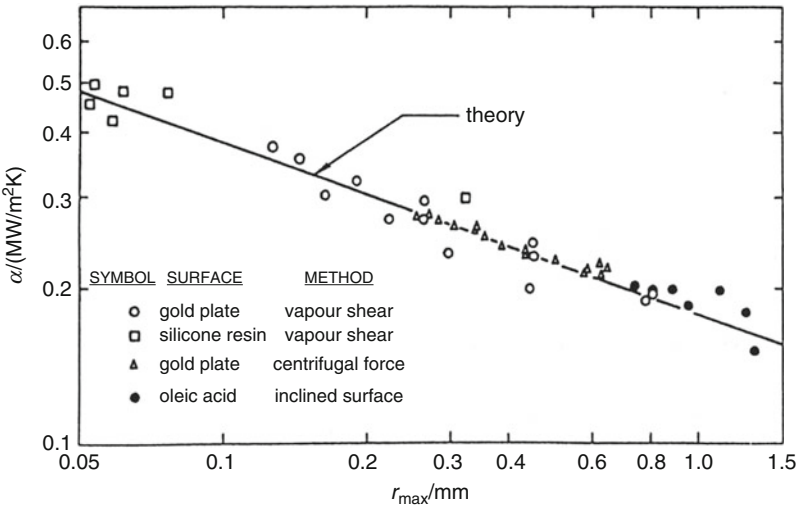

Fig. 23 Dependence of heat-transfer coefficient on maximum drop size (Rose (1988b). Comparison of theory with experimental data (Tanasawa 1974; Tanasawa et al. 1974)

With somewhat different values of the constants, comparisons with data for dropwise condensation of ethylene glycol (Stylianou and Rose 1982) and mercury (Niknejad and Rose 1984) have been given.

6.2.6 Dropwise Condensation on Horizontal Tubes

The forgoing discussion relates to dropwise condensation on vertical plane surfaces. Experiments with inclined surfaces for steam at atmospheric pressure (Citakoglu and Rose 1969) in which the angle of inclination ranged from horizontal face down to near-horizontal face up indicated that the heat-transfer coefficient was quite weakly dependent on inclination of the condensing surface over much of the range. On the basis of these data, it was suggested that the average coefficient for a horizontal tube might be around 80% that of a vertical plane surface as calculated from the foregoing theory.

6.3 Transition

Transition from dropwise to film condensation, analogous to that of nucleate to film boiling, occurs at sufficiently high heat flux. Wilmshurst and Rose (1974) reported measurements for aniline and nitrobenzene when transition occurred at heat fluxes between about 0.1 and 0.2 MW/m^2 and vapor-surface temperature differences around 20 K. Tanasawa and Utaka (1983), using liquid nitrogen as coolant, observed transition for steam to occur at a heat flux of around 10 MW/m^2 and vapor-surface temperature difference around 20 K. The theory described above gives a heat flux of around 9 MW/m^2 at this temperature difference.

6.4 Conclusion

Reliable experimental data, not vitiated by effects of noncondensing gas, are well predicted by theory and show that the heat-transfer coefficient increases with increasing vapor-surface temperature difference and decreases with pressure. For dropwise condensation of steam, Eq. 79 gives an adequate representation of the heat flux-temperature difference relationship for practical purposes. The experiments and theory relate to promoters where the contact angle is not far for 90°. For significantly larger contact angles, such as seen in the more recent investigations with nanostructured surfaces and for condensation of mercury, the form of the drop size distribution might be expected to be different to that given by Eqs. 64, 65, and 66. For contact angles less than or equal to 90°, coalescence occurs when the base circles of drops come into contact, while for larger contact angles, this occurs when parts of the curved surfaces come into contact. It may be noted that for contact angles approaching 180°, much of the surface would be essentially adiabatic (single-phase heat-transfer from subcooled vapor). For zero contact angle, film condensation is obtained, so that an optimum contact angle exists which may not be far from 90°. For "super-hydropic" surfaces where droplets spring from the surface, there is no sweeping effect of sliding droplets.

7 Cross-References

- ▶ Boiling and Two-Phase Flow in Narrow Channels
- ▶ Boiling on Enhanced Surfaces
- ▶ Flow Boiling in Tubes
- ▶ Fundamental Equations for Two-Phase Flow in Tubes
- ▶ Heat Pipes and Thermosyphons
- ▶ Internal Annular Flow Condensation and Flow Boiling: Context, Results, and Recommendations
- ▶ Mixture Boiling
- ▶ Nucleate Pool Boiling
- ▶ Phase Change Materials
- ▶ Single- and Multiphase Flow for Electronic Cooling
- ▶ Transition and Film Boiling

References

Adamek T, Webb RL (1990) Prediction of film condensation on horizontal integral fin tubes. Int J Heat Mass Transf 33:1721–1735

Ali H, Wang HS, Briggs A, Rose JW (2013) Effect of vapor velocity and pressure on Marangoni condensation of steam-ethanol mixtures on a horizontal tube. J Heat Transf 135:091602-1

Bandhauer TM, Agarwal A, Garimella S (2006) Measurements and modelling of condensation heat transfer coefficients in circular microchannels. Trans ASME J Heat Transf 128:1050–1059
Beatty KO, Katz DL (1948) Condensation of vapors on outside of finned tubes. Chem Eng Prog 44:55–70
Berman LD (1969) Determination of mass transfer coefficient in calculations on condensation of steam containing air. Teploenergetika 16:68–71
Briggs A, Rose (1994) Effect of fin efficiency on a model for condensation heat transfer on a horizontal integral fin tube. Int J Heat Mass Transf 37(Suppl):457–463
Briggs A, Rose JW (1998) Effects of interphase matter transfer and non-uniform wall temperature on a model for condensation on low-finned tubes. I J Transp Phenom 1:41–49
Cavallini A, Del Col D, Doretti L, Matkovic M, Rossetto L, Zilio C (2005) A model for condensation inside minichannels. In: Proceedings of the ASME National heat transfer conference, San Francisco, paper HT2005-72528
Cess RD (1960) Laminar film condensation on a flat plate in the absence of a body force. Z Angew Math Phys 11:426–433
Chen MM (1961a) Analytical solution of laminar film condensation: part 1 flat plates. Trans ASME J Heat Transf 83:48–54
Chen MM (1961b) Analytical solution of laminar film condensation: part 2 single and multiple horizontal tubes. Trans ASME J Heat Transf 83:55–60
Citakoglu E, Rose JW (1968) Dropwise condensation – some factors influencing the validity of heat-transfer measurements. Int J Heat Mass Transf 11:523–537
Citakoglu E, Rose JW (1969) Dropwise condensation – the effect of surface inclination. Int J Heat Mass Transf 12:645–651
Denny VE, Mills AF (1969) Laminar film condensation of a flowing vapor on a horizontal cylinder at normal gravity. Trans ASME 91C:495–501
Enright R, Miljkovic N, Alverado JL, Kim K, Rose JW (2014) Dropwise condensation on micro- and nanostructured surfaces. Nanoscale Microscale Thermophysical Eng 18(3):223–250
Fatica N, Katz DL (1949) Dropwise condensation. Chem Eng Prog 45:661–674
Fujii T, Uehara H (1972) Laminar filmwise condensation on a vertical surface. Int J Heat Mass Transf 15:217–233
Fujii T, Uehara H, Kurata C (1972a) Laminar filmwise condensation of a flowing vapour on a horizontal cylinder. Int J Heat Mass Transf 15:235–246
Fujii T, Uehara H, Oda K (1972b) Film condensation on a surface with uniform heat flux and body force convection. Heat Transf Jpn Res 4:76–83
Fujii T, Uehara H, Mihara K, Kato K (1977) Forced convection condensation in the presence of non-condensables – a theoretical treatment for two-phase laminar boundary layer. Univ Kyushu Res Inst Ind Sci Rep 66:53–80
Graham C (1969) The limiting mechanisms of dropwise condensation. PhD thesis, M.I.T
Honda H, Nozu S (1987) A prediction method for heat transfer during film condensation on horizontal low integral-fin tubes. Trans ASME J Heat Transf 109:218–225
Honda H, Nozu S, Mitsumori K (1983) Augmentation of heat transfer on horizontal finned tubes by attaching a porous drainage plate. Proc ASME-JSME Therm Eng Joint Conf 3:289–296
Ishiyama T, Yano T, Fujikawa S (2004a) Molecular dynamics study of kinetic boundary condition at an interface between argon vapor and its condensed phase. Phys Fluids 16:2899–2906
Ishiyama T, Yano T, Fujikawa S (2004b) Molecular dynamics study of kinetic boundary condition at an interface between a polyatomic vapor and its condensed phase. Phys Fluids 16:4713–4726
Ishiyama T, Yano T, Fujikawa S (2005) Kinetic boundary condition at a vapor-liquid interface. Phys Rev Lett 95:084504
Karkhu VA, Borovkov VP (1971) Film condensation of vapor at finely-finned horizontal tubes. Heat Transf Sov Res 3:183–191
Kim S-M, Mudawar I (2012) Flow condensation in parallel microchannels – part 2: heat transfer results and correlation technique. Int J Heat Mass Transf 55:984–994
Kim S-M, Kim J, Mudawar I (2012) Flow condensation in parallel microchannels – part 1: experimental results and pressure drop correlations. Int J Heat Mass Transf 55:971–983

Knudsen M (1915) Die Maximale Verdampfungsgeschwindigkeit des Quecksilbers. Ann Phys Chem 47:697–708
Koh JC (1962) Laminar film condensation of condensable gases and mixtures on a flat plate. Proc 4th USA Nat Cong Appl Mech 2:1327–1336
Koh JC, Sparrow EM, Hartnett JP (1961) The two-phase boundary layer in laminar film condensation. Int J Heat Mass Transf 2:69–82
Koyama S, Kuwahara K, Nakashita K (2003b) Condensation of refrigerant in a multi-port channel. In: 1st international conference on microchannels & minichannels, Rochester, pp 193–205
Koyama S, Kuwahara K, Nakashita K, Yamamoto K (2003a) An experimental study on condensation of refrigerant R134a in a multi-port extruded tube. Int J Refrig 24:425–432
Labuntsov DA (1967) An analysis of evaporation and condensation processes. Teplofiz Vysok Temp 5:647–653
Labuntsov DA, Kryukov AP (1979) Analysis of intensive evaporation and condensation. Int J Heat Mass Transf 22:989–1002
Labuntsov DA, Muratova TM (1969) Influence of motion on evaporation and condensation. Teplofiz Vysok Temp 7:1146–1150
Le Fevre EJ (1964) See appendix G of Rose (1964)
Le Fevre EJ, Rose JW (1964) Heat-transfer during dropwise condensation of steam. Int J Heat Mass Transf 7:272–273
Le Fevre EJ, Rose JW (1965) An experimental study of heat transfer by dropwise condensation. Int J Heat Mass Transf 8:1117–1133
Le Fevre EJ, Rose JW (1966) A theory of heat transfer by dropwise condensation. Proc 3rd Int Heat Transf Conf 2:362–375
Lee WC, Rose JW (1982) Film condensation on a horizontal tube – effect of vapour velocity. Proc 7th Int Heat Transf Conf 5:101–106
Masuda H, Rose (1987) Static configuration of liquid film on horizontal tubes with low radial fins. Proc R Soc Lond A410:125–139
Meland R, Frezzotti A, Ytrehus T, Hafskjold B (2004) Nonequilibrium molecular-dynamics simulation of net evaporation and net condensation, and evaluation of the gas-kinetic boundary condition at the interface. Phys Fluids 16:223–243
Memory SB, Rose JW (1986) Film condensation of ethylene glycol on a horizontal tube at high vapour velocity. Proc 8th Int Heat transfer Conf, San Francisco 4:1607–1612
Memory SB, Rose JW (1991) Free convection laminar film condensation on a horizontal tube with variable wall temperature. Int J Heat Mass Transf 34:2775–2778
Michael AG, Rose JW, Daniels LC (1989) Forced convection condensation on a horizontal tube. Trans ASME J Heat Transfer 111:792–797
Mijlkovic N, Preston DJ, Wang EN (2016) Recent developments in altered wettability for enhancing condensation. In: Thome JR, Kim J (eds) Encyclopaedia of two-phase heat transfer and flow II, special topics and applications 3 special topics in condensation. World Scientific, Singapore, pp 85–131
Mills AF, Tan C, Chung DK (1974) Experimental study of condensation from steam-air mixtures flowing over a horizontal tube: overall condensation rates. Proc 5th Int Heat Transf Conf Tokyo 5:20–23
Minkowicz WJ, Sparrow EM (1966) Condensation heat transfer in the presence of noncondensables, interfacial resistance, superheating, variable properties and diffusion. Int J Heat Mass Transf 9:1125–1144
Nagayama G, Tsuruta T (2003) A general expression for the condensation coefficient based on transition state theory and molecular dynamics simulation. J Chem Phys 118:1392–1399
Niknejad J, Rose JW (1981) Interphase matter transfer – an experimental study of condensation of mercury. Proc R Soc London A 378:305–327
Niknejad J, Rose JW (1984) Comparisons between experiment and theory for dropwise condensation of mercury. Int J Heat Mass Transf 27:2253–2257

Nusselt W (1916) Die Oberflachencondensation des Wassserdampfes Z. Vereines Deutsch Ing 60:569–575
Rahbar S, Rose JW (1984) New measurements for forced convection film condensation. 1st UK Natl Conf Heat Transf 1:609–632
Rifert VG (1980) A new method for calculating rates of condensation on finned tubes. Heat Transfer Sov Res 12:142–147
Rose JW (1964) Dropwise condensation of steam on vertical planes. PhD thesis, London University
Rose JW (1967) On the mechanism of dropwise condensation. Int J Heat Mass Transf 10:755–762
Rose JW (1969) Condensation of a vapour in the presence of a non-condensing gas. Int J Heat Mass Transf 12:233–237
Rose JW (1976) Further aspects of dropwise condensation theory. Int J Heat Mass Transf 19:1363–1370
Rose JW (1980) Approximate equations for forced convection condensation in the presence of a non-condensing gas on a flat plate and horizontal tube. Int J Heat Mass Transf 23:539–546
Rose JW (1984) Effect of pressure gradient in forced convection film condensation on a horizontal tube. Int J Heat Mass Transf 27:39–47
Rose JW (1988a) Fundamentals of condensation heat transfer: laminar film condensation. JSME Int J Ser 2(31):357–375
Rose JW (1988b) Some aspects of condensation heat transfer theory. Int Com Heat Mass Transf 15:449–473
Rose (1989) A new interpolation formula for forced convection condensation on a horizontal surface. Trans ASME 111:818–819
Rose JW (1994) An approximate equation for the vapor-side heat-transfer coefficient for condensation on low-finned tubes. Int J Heat Mass Transf 37:865–875
Rose JW (1998a) Interphase matter transfer the condensation coefficient and dropwise condensation. In: Proceedings of the 11th international heat transfer conference, vol 1, Kyongju, 23–28 Aug 1998, pp 89–104
Rose JW (1998b) Condensation heat transfer fundamentals. Trans IChemE 76(part a):143–152
Rose JW (2000) Accurate approximate equations for intensive subsonic evaporation. Int J Heat Mass Transf 43:3869–3875
Rose JW (2002) Dropwise condensation theory and experiment: a review. Proc Instn Mech Eng Part A J Power Energy 251:115–170
Rose JW, Glicksman LR (1973) Dropwise condensation – on the distribution of drop sizes. Int J Heat Mass Transf 16:411–425
Schmidt E, Schurig W, Sellschopp W (1936) Versuche uber die Kondensation in Film- und Tropfenform. Tech Mech Thermodynamik 1:53–63
Schrage RW (1953) A theoretical study of interphase mass transfer. Columbia University Press, New York
Shekriladze IG, Gomelauri VI (1966) The theoretical study of laminar film condensation of a flowing vapour. Int J Heat Mass Transf 9:581–591
Sone Y, Onishi Y (1973) Kinetic theory of evaporation and condensation. J Phys Soc Jpn 35:1773–1776
Sparrow EM, Gregg JL (1959) A boundary layer treatment of laminar film condensation. J Heat Transfer 81:13–23
Sparrow EM, Lin SH (1964) Condensation in the presence of a non-condensing gas. J Heat Transfer 86:430–436
Sparrow EM, Minkowycz WM, Saddy M (1967) Forced convection condensation in the presence of non-condensables and interface resistance. Int J Heat Mass Transf 10:1829–1845
Stylianou S, Rose JW (1980) Dropwise condensation on surfaces having different thermal conductivity. J Heat Transfer 102:477–482
Stylianou S, Rose JW (1982) Dropwise condensation of ethane diol. PhysicoChem Hydrodyn 3:199–213

Su Q, Yu GX, Wang HS, Rose JW (2009) Microchannel condensation: correlations and theory. Int J Refrig 32:1149–1152
Tanaka H (1975) A theoretical study on dropwise condensation. J Heat Transfer 97:72–98
Tanasawa H (1974). Critical size of departing drops. In: Proceedings of the 5th international heat transfer conference, vol 7, Tokyo, 3–7 Sept 1974, p 188
Tanasawa I, Ochiai J (1973) Experimental study on heat transfer during dropwise condensation. Bull Jpn Soc Mech Eng 16:1184–1197
Tanasawa I, Ochiai J, Utaka Y, Enya S (1974) Proceedings of the 11th Japan heat transfer symposium, p 229 (in Japanese)
Tasnasawa I, Utaka Y (1983) Measurement of condensation curves for dropwise condensation of steam at atmospheric pressure. J Heat Transf 105(3):633–638
Tsuruta T, Nagayama G (2005) A microscopic formulation of condensation coefficient and interface transport phenomena. Energy 30(6):795–805
Umur A, Griffith P (1965) Mechanism of dropwise condensation. J Heat Transf 87:275–282
Wang HS, Rose JW (2005) A theory of film condensation in horizontal noncircular section microchannels. Trans ASME J Heat Transf 127:1096–1105
Wang HS, Rose JW (2011) Theory of heat transfer during condensation in microchannels. Int J Heat Mass Transf 54:2525–2534
Wang ZJ, Chen M, Guo ZY (2003) A molecular study of the liquid-vapor interphase transport. Microscale Thermophys Eng 7:275–289
Wanniarachchi AS, Marto PJ, Rose JW (1985) Film condensation of steam on horizontal finned tubes. Effect of fin spacing, thickness and height (1985). Multiphase flow and heat transfer. ASME HTD 47:93–99
Webb RL, Rudy TM, Kedzierski MA (1985) Prediction of condensation coefficient on horizontal integral-fin tubes. Trans ASME J Heat Transfer 107:369–376
Wenzel H (1957) Versuche über Tropfenkondensation. Allg Wärmetech 8:53–59
Wilmshurst R, Rose JW (1970) Dropwise condensation – further heat-transfer measurements. In: Proceedings of the 4th international heat-transfer conference, Versailles, Paper Cs 1.4
Wilmshurst R, Rose JW (1974) Dropwise and filmwise condensation of aniline, ethane diol and nitrobenzene. In: Proceedings of the 5th international heat-transfer conference, Tokyo. Japan Soc Mech Eng, pp 269–273
Ytrehus T, Alvestad J (1981) A Mott-Smith solution for non-linear condensation. In: Fisher SS (ed) Rarefied Gas Dynamics, Prog. Astro. and Aero.74, pp 330–345
Zhou Y-Q, Rose (1996) Effect of two-dimensional conduction in the condensate film on laminar film condensation on a horizontal tube with variable wall temperature. Int J Heat Mass Transf 39:3187–3191